Field Relationships, Geochemistry, Zircon Ages and Evolution of a Late Archaean to Palaeoproterozoic Lower Crustal Section in the Hengshan Terrain of Northern China

A. KRÖNER[1], S.A. WILDE[2], P.J. O'BRIEN[3], Jianghai LI[4],
C.W. PASSCHIER[1], N.P. WALTE[1] and LIU Dunyi[5]

1 *Institut für Geowissenschaften, Universität Mainz, D-55099 Mainz, Germany;*
E-mail: kroener@mail.uni-mainz.de
2 *School of Applied Geology, Curtin University of Technology*
GPO Box U1987, Perth, WA 6845, Australia
3 *Institut für Geowissenschaften, Universität Potsdam, Postfach 601553,*
D-01553 Potsdam, Germany
4 *Department of Geology, Peking University, Beijing 109009, China*
5 *Chinese Academy of Geological Sciences, 26 Baiwanzhuang Road, Beijing 100037, China*

Abstract   The Hengshan complex forms part of the central zone of the North China Craton and consists predominantly of ductilely-deformed late Archaean to Palaeoproterozoic high-grade, partly migmatitic, granitoid orthogneisses, intruded by mafic dykes of gabbroic composition. Many highly strained rocks were previously misinterpreted as supracrustal sequences and represent mylonitized granitoids and sheared dykes. Our single zircon dating documents magmatic granitoid emplacement ages between 2.52 Ga and 2.48 Ga, with rare occurrences of 2.7 Ga gneisses, possibly reflecting an older basement. A few granitic gneisses have emplacement ages between 2.35 and 2.1 Ga and show the same structural features as the older rocks, indicating that the main deformation occurred after ~2.1 Ga. Intrusion of gabbroic dykes occurred at ~1920 Ma, and all Hengshan rocks underwent granulite-facies metamorphism at 1.88–1.85 Ga, followed by retrogression, shearing and uplift.

We interpret the Hengshan and adjacent Fuping granitoid gneisses as the lower, plutonic, part of a late Archaean to early Palaeoproterozoic Japan-type magmatic arc, with the upper, volcanic part represented by the nearby Wutai complex. Components of this arc may have evolved at a continental margin as indicated by the 2.7 Ga zircons. Major deformation and HP metamorphism occurred in the late Palaeoproterozoic during the Lüliang orogeny when the Eastern and Western blocks of the North China Craton collided to form the Trans-North China orogen. Shear zones in the Hengshan are interpreted as major lower crustal discontinuities post-dating the peak of HP metamorphism, and we suggest that they formed during orogenic collapse and uplift of the Hengshan complex in the late Palaeoproterozoic (<1.85 Ga).

Key words: Archaean to Palaeoproterozoic geology, zircon age, Hengshan terrain, North China Craton

1 Introduction

The well exposed Hengshan terrain of the North China Craton (NCC) is situated in northern Shanxi Province, about 250 km WSW of Beijing (Fig. 1), and is one of the classical areas of Archaean to Palaeoproterozoic geology of China. It is separated from the Wutai Mts. by the broad valley of the Hutuo River and is made up of the Heng Mts., extending in a broad NE-SW trending belt and bounded by the valleys of the Sanggan and Hutou Rivers (Fig. 1). The Heng Mts. constitute a typical high-grade gneiss terrain with complexly deformed layered and migmatized ortho- and minor paragneisses (Li and Qian, 1994, and references therein) and, until recently, was believed to have been deformed and metamorphosed in the late Archaean (Li and Qian, 1994; Tian et al., 1996; Li et al., 1997; Kusky and Lee, 2003). Of particular interest in the Hengshan are well

studied mafic granulites (Wang et al., 1991), derived from gabbroic mafic dykes and previously believed to result from a late Archaean high-pressure (HP) metamorphic event (Li and Qian, 1994; Li et al., 1997, 1998a,b; Zhao et al., 1999b; Kusky and Lee, 2003).

Some of the new ideas resulting from our recent work in the Hengshan terrain can be summarized as follows: (1) The mafic gneisses in the Hengshan are strongly deformed gabbroic dykes that were emplaced at ca. 1920 Ma (Kröner et al., 2005b) and experienced their HP metamorphism about 1850–1880 Ma ago (Kröner et al., 2000, 2001; O'Brien et al., 2005). This is in line with the metamorphic history of adjacent regions in the NCC (Guo et al., 1994; Wilde et al., 1998; Zhao et al., 2004) and supports the concept of a major Palaeoproterozoic tectono -thermal event in the central zone of the NCC , in the Chinese literature also known as the Lüliang orogeny (Ma
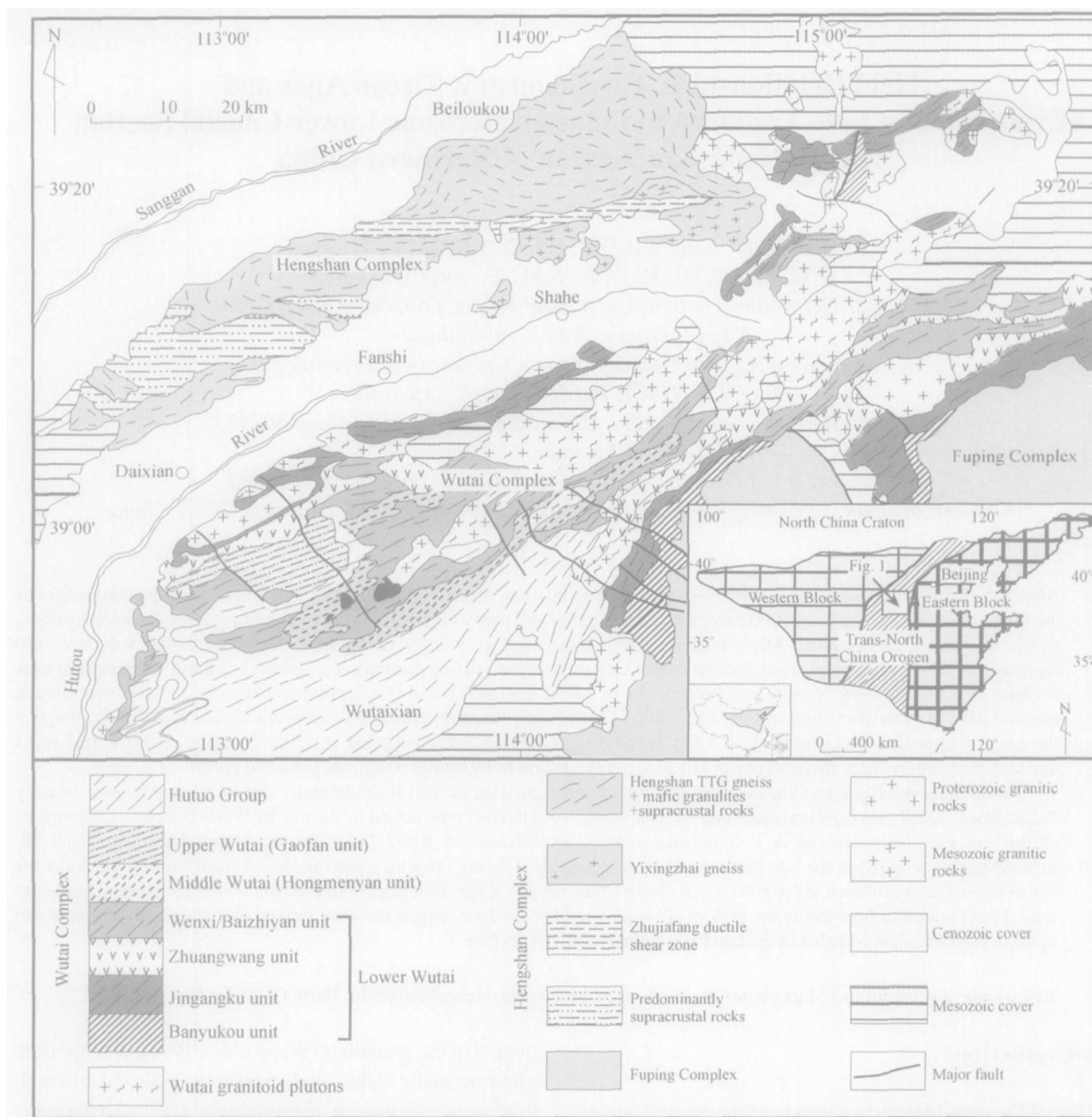
Fig. 1. Overview map of the Hengshan-Wutai-Fuping Archaean to Palaeoproterozoic terrain showing major rock types and location within the Trans-North China orogen of the North China Craton (from Kröner et al., 2005b).

and Bai, 1998). (2) The presence of ductilely deformed Palaeoproterozoic granitoid gneisses and ~1.92 Ga mafic dykes in the Hengshan indicates that the main deformation in the Heng Mts. is not Archaean in age (Li et al., 1998a) but Palaeoproterozoic, supporting models suggesting collision of the Western and Eastern blocks of the NCC along a broad belt named the Trans-North China Orogen (see Fig. 1, inset; Zhao et al., 2001). (3) The Hengshan and geologically similar and geographically adjacent Fuping high-grade gneisses (Fig. 1) may be the lower crustal, ductilely deformed equivalents of the upper crustal Wutai greenstone terrain farther east and may represent the root zone of the magmatic arc (Li and Qian, 1994; Kröner et al., 2001; 2002, 2005a). Models invoking late Archaean cratonization in North China (Li et al., 2000a; Kusky and Li, 2003) are not supported by the current data, as will be shown below.

This contribution summarizes field observations and reports geochemical data and single zircon ages for the Hengshan terrain to provide constraints for the above new tectonic hypotheses.
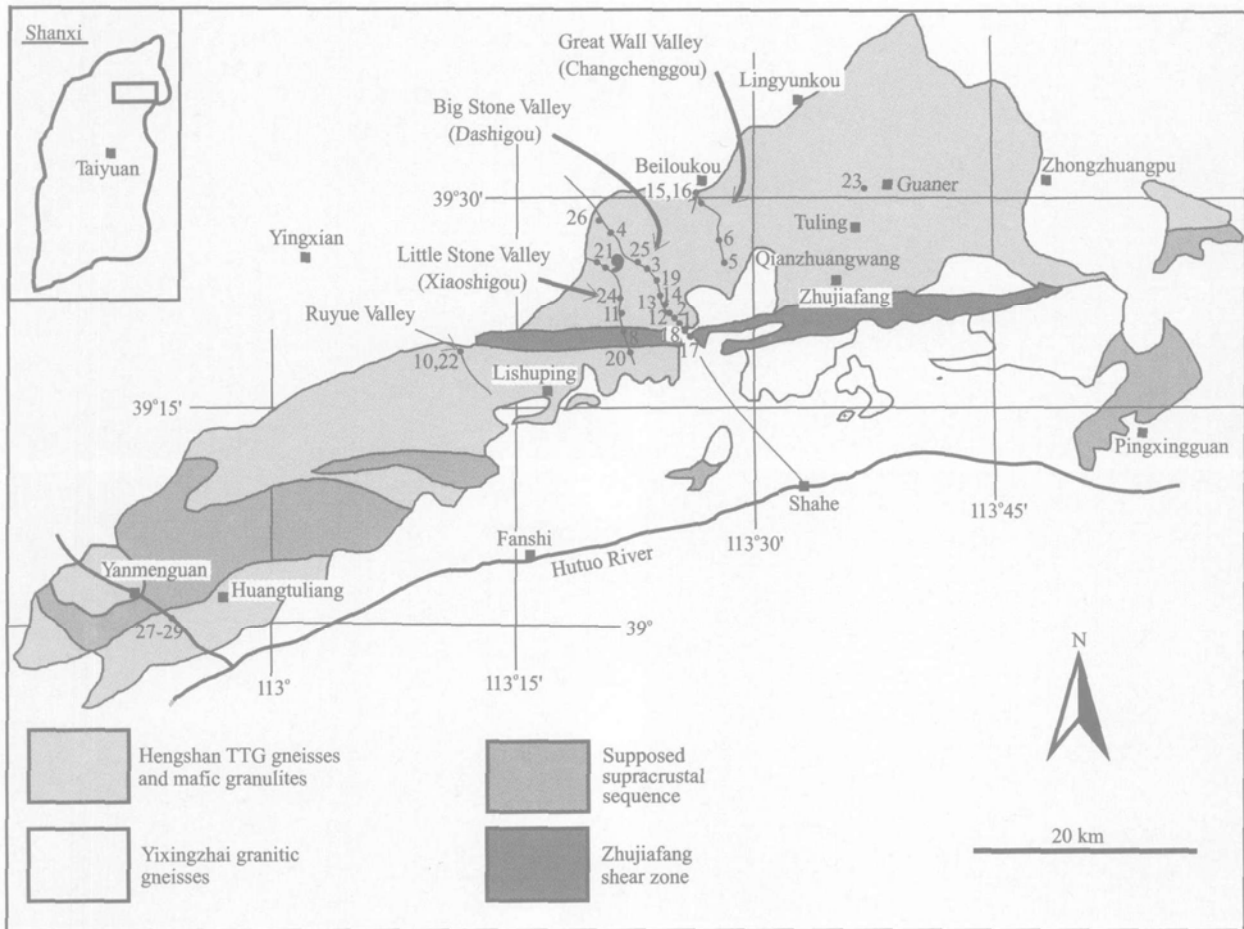
Fig. 2. Simplified map of the Hengshan Complex showing main rock types, the three valleys in which samples were taken, and location of villages and towns.

2 Field Relationships, Structure and Metamorphic Evolution of the Hengshan Terrain

The gneisses and migmatites of the Hengshan have been described in detail by Li and Qian (1994) and Tian et al. (1996) and are particularly well exposed in three NW-SE trending valleys named Great Wall Valley (Changchenggou), Big Stone Valley (Dashigou) and Little Stone Valley (Xiaoshigou) (Fig. 2). The asphalt road between the towns of Shahe and Yingxian follows Big Stone Valley and has almost continuously fresh, blasted exposures. This is also the case along the asphalt road from Taihelingkou to Xinguanwu along a NW-SE traverse across the southern Hengshan via Yanmengguan (Fig. 2).

The majority of rocks are ductilely deformed, layered orthogneisses of tonalitic, trondhjemitic, granodioritic and granitic composition (TTGG-suite, Li and Qian, 1994), similar to "grey gneisses" in Archaean terrains elsewhere in the world (Fig. 3a), and were collectively named

Hengshan grey gneisses or Hengshan complex (Tian, 1986). These rocks are extensively migmatized, as particularly well displayed along the asphalt road in Big Stone Valley, and some of the migmatized zones show evidence of extensive in-situ melting and advanced anatexis, generating reddish granites (Fig. 3b). Several of the granitic to granodioritic gneisses interlayered with the more mafic gneiss varieties are considered to be the result of anatexis of older tonalitic rocks (Li and Qian, 1994). The compositional layering in the TTGG gneisses ranges from dark, hornblende-rich dioritic to tonalitic compositions to K-feldspar-dominated leucocratic granitoid varieties and was probably produced by a mechanism of ductile flattening as described by Myers (1978) and Passchier et al. (1990).

Rare fine-grained, felsic gneisses described as biotite leptynites and interpreted as greywacke in the Chinese literature (e.g., Li and Qian, 1994; Tian et al., 1996) are interlayered with the granitoid gneisses and, on the basis of zircon morphology and age (see below), we consider these to be derived from felsic volcanic rocks such as
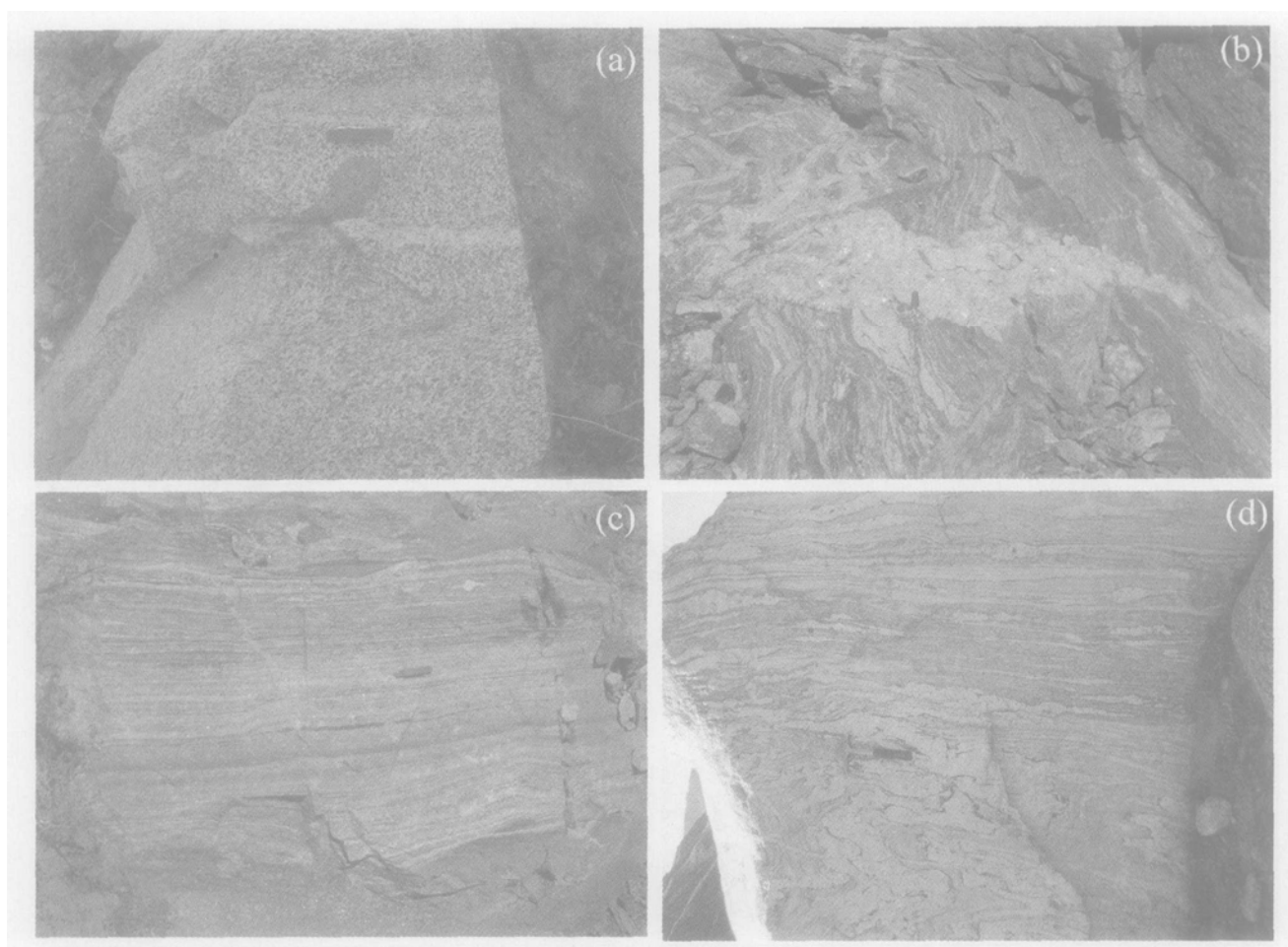
Fig. 3. Field photographs. (a) Typical tonalite with incipient shear zones N of Shahe town (Yixingzhai gneiss) and south of the Zhujiafang shear zone. This rock has a SHRIMP zircon age of 2513±15 Ma (S.A. Wilde, reported in Kröner et al., 2002). (b) Migmatite showing deformed in-situ melt aggregates and cross-cutting pegmatitic material. Roadcut in NW-part of Big Stone Valley. (c) Well layered trondhjemitic gneiss in shear zone of Little Stone Valley. Note K-feldspar sigma-clast in upper right part and thin, boudinaged mafic layer (mafic dyke) in middle part of photo. (d) Migmatitic, granodioritic gneiss with strong strain gradient; upper part shows high-strain fabric with flattened and boudinaged layers; Great Wall Valley.

dacites and rhyodacites. Other Al-rich gneisses locally containing kyanite are undoubtedly of sedimentary origin as are quartzites and thin layers of BIF. The sedimentary assemblage suggests shallow-water deposition, and this is similar to many other Archaean to Palaeoproterozoic high-grade terrains such as eastern Hebei Province in China and the Limpopo belt of southern Africa (Kröner, 1998).

Within the gneisses there occur numerous boudins and lensoid layers of dark mafic gneisses or amphibolites (Fig. 4a, b) predominantly consisting of an assemblage of hornblende, plagioclase, garnet, clinopyroxene, quartz and rutile, which commonly exhibit HP metamorphic assemblages in their cores that are downgraded along the margins (e.g., Wang et al., 1991; Li et al., 1998a; Walte, 2001; O'Brien et al., 2005). In rare cases, and in particular in low-strain zones such as south of the major Zhujiafang shear zone at the southern end of Little Stone Valley, a

typical gabbroic primary igneous fabric is preserved. A dyke in upper Big Stone Valley dated by Kröner et al. (2005b) at 1914±2 Ma still displays primary magmatic layering. There can be no doubt that these amphibolites are remnants of mafic dykes that originally intruded into the granitoid rocks as can still be observed at a few localities in low strain zones. Kröner et al. (2005b) dated igneous zircons from two samples of gabbroic dykes in Big Stone Valley at ~1915 Ma and interpreted this age to reflect emplacement of the dykes.

Ductile deformation has later rotated these dykes into parallelism with the layering in the enclosing gneisses (cf. Myers, 1978; see Fig. 4d) and, at the same time, caused boudinage (Fig. 4b). The resulting pattern is essentially the same as in high-grade gneiss terrains in SW Greenland, in the Lewisian complex of Scotland, in the Ancient Gneiss complex of Swaziland, the Limpopo belt of southern
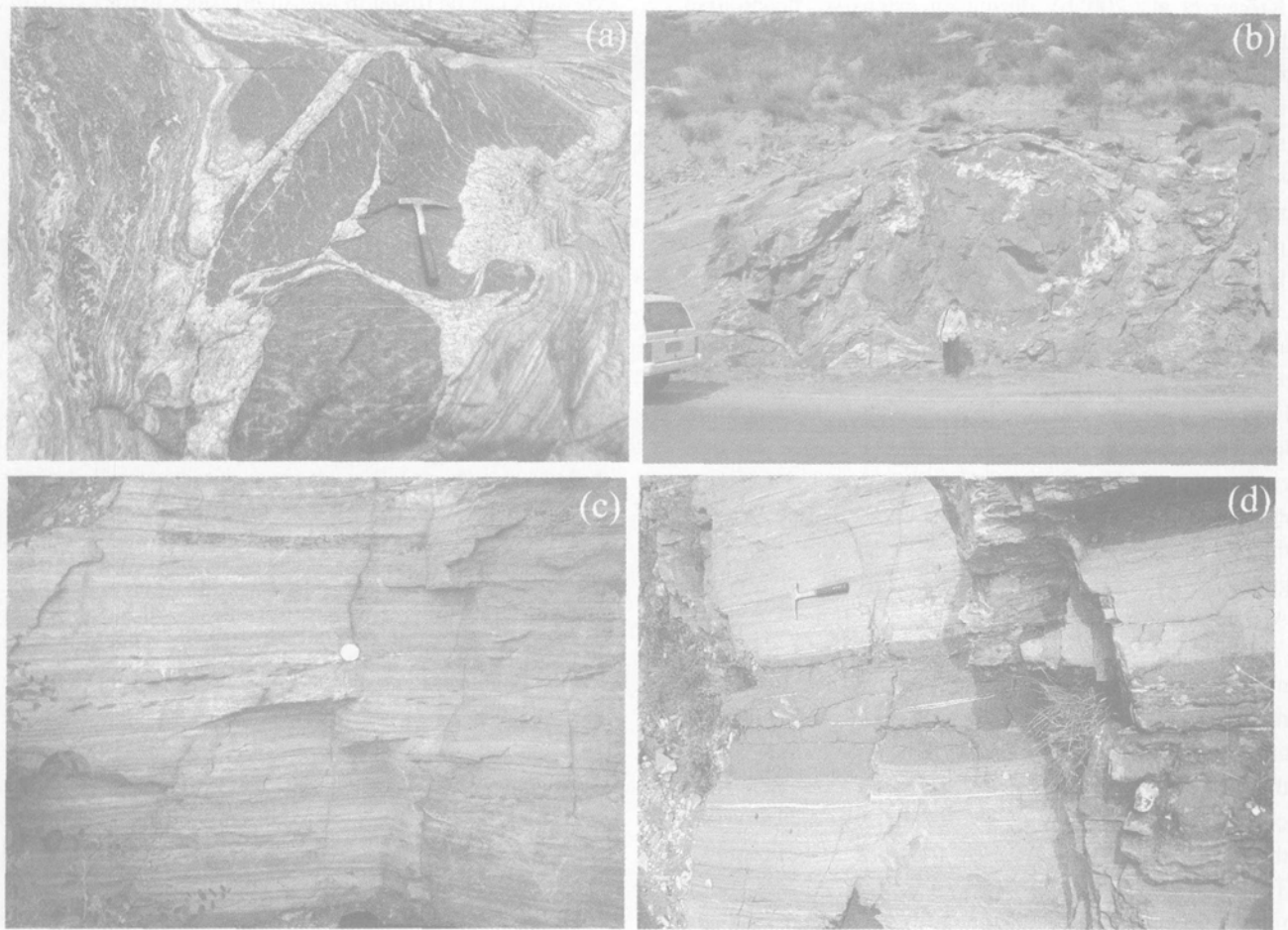
Fig. 4. Field photographs. (a) Disrupted gabbroic dyke fragments enclosed in TTG gneiss and intruded by granitic melt which cuts an older fabric; Roadcut in Big Stone Valley. (b) Large boudin of metagabbro enclosed in granitoid gneiss. Roadcut in Big Stone Valley. (c) Ductilely sheared granitoid gneiss with fine banding resembling supracrustal sequence; Zhujiafang shear belt S of Zhujiafang village. (d) Ductile mylonite zone with finely layered granitoid gneiss and foliated gabbroic dyke in centre. Zhujiafang shear zone in valley S of Zhujiafang village.

Africa, the Archaean gneisses of the Slave Province of Canada and the Archaean terrain of the northern Yilgarn craton of Western Australia (see Goodwin, 1991, for further examples). In all these cases, the amphibolitic layers and boudins are part of original dyke swarms indicating major extensional events in the history of the complexes in which they occur. The mafic dykes have been of particular interest in recent years since they contain metamorphic mineral assemblages recording a HP event with T up to 900°C and P up to 16 kbar (for summary of data and literature see Zhai, 1997; Zhao et al., 2001; O'Brien et al., 2005).

At many localities the Hengshan gneisses are affected by strong ductile deformation in well-defined ENE-WSW striking shear zones that cut across the regional layering/foliation and led to complete refoliation (Fig. 4c). These high-grade shear zones (T up to 780°C, P up to 8 kbar, Walte, 2001) are from several mm to several hundred metres in width and frequently contain shear-sense indicators pointing to dextral movement (Fig. 3c). In at least three broad shear zones examined by us the orthogneisses and gabbroic dykes have been extensively refoliated into a finely banded assemblage of upper amphibolite- to greenschist-facies gneisses and/or schists (Figs. 4c, d) that have previously been misinterpreted as supracrustal rocks and erroneously been assigned to the Wutai low-grade greenstone assemblage that is exposed in the nearby Wutai Mountain range (e.g., Li and Qian, 1994; Tian, 1996).

The Hengshan gneisses experienced several phases of deformation, but much of the early structural history of these rocks was probably obliterated during intense ductile shearing that produced a penetrative layering. Rare tight intrafolial folds within this layering record the oldest structures seen. The layering itself was produced after emplacement of the mafic dykes, i.e. after 1915 Ma ago

(Kröner et al., 2005b), during an extensive, penetrative ductile event under lower crustal conditions. The dykes were also affected by this phase of deformation, leading to rotation, severe flattening and boudinage. The layering itself is commonly folded into isoclinal folds associated with a strong stretching mineral lineation. This folding becomes irregular around large mafic boudins because of a marked ductility contrast between the layered gneisses and the disrupted dyke material.

The oldest structure visible in the field is a S_1 foliation in low-strain zones south of the major shear zone, particularly in a road-cut north of the village of Yixingzhai. Here, a steeply foliated, syntectonic, coarse-grained tonalitic to granodioritic rock (Fig. 3a) yielded a SHRIMP zircon age of 2513 ± 15 Ma (S.A. Wilde, reported in Kröner et al., 2002), and it is obvious from field relationships that the penetrative fabric formed during crystallization of the granitoid melt. This fabric is therefore clearly of late Archaean origin.

Within the high-grade, ductilely deformed terrain, a mineral foliation (S_2) is locally preserved in boudinaged remnants of the mafic dykes. S_2 is defined by elongated crystals of greenish former sodium-rich clinopyroxene that reacted to a fine intergrowth of secondary clinopyroxene and plagioclase (O'Brien et al., 2005). S_2 therefore formed during high pressure metamorphism. This implies that all deformation visible outside of the mafic boudins is connected to exhumation and the retrograde history of the Hengshan.

D_3 is the main phase of deformation under high-grade conditions and produced the distinctive gneissic layering S_3, followed by partial melting of variable intensity. This erased all older structures except for relicts in the mafic boudins. Intensely foliated D_3-high strain zones alternate with less deformed lower strain zones (e.g. Fig. 3d), showing a foliation strike from N-S and NE-SW in the North to E-W in the central and southern part of the range (Zhujiafang unit, Fig. 2). D_3 deformation led to boudinage of the northern mafic granulites and was coeval with partial melting and retrogression to amphibolite-facies within the boudins. The partial melts tend to collect in the boudin necks and connect the individual boudins with a thin trace of white melt, sometimes over long distances.

The fourth phase of deformation (D_4) is presented by several kilometre-wide E-W steep, transcurrent shear zones, such as the Zhujiafang belt (Fig. 2), that extend for the full length of the Hengshan. These shear zones show a dextral sense of shear, with a local dip-slip component. The change in strike of S_3 in the northern Hengshan is probably an effect of dextral shear on these major shear zones. In the gneisses near the shear zone, D_4 is locally recorded as tight folding of the D_3 foliation. Similar exposures can be found in low strain zones in the centre of the Zhujiafang shear zone, therefore indicating that the Zhujiafang unit simply represents strongly sheared Hengshan gneisses mainly of magmatic origin. The shear zones record a history of deformation from hornblende-stability at upper amphibolite-facies conditions to greenschist facies ultramylonite and pseudotachylite, recording the transition to brittle deformation. The dextral sense of shear is recorded by asymmetric feldspar clasts, deformation of syn-D_4 intruded pegmatite dykes, and C´ shear bands found in thin sections of ultramylonite.

In the western part of the Hengshan, and particularly well exposed in road cuts SE of Yanmenguan (Fig. 2), steeply dipping and weakly deformed dolerite dykes with chilled margins cut S_3 but are overprinted statically by low pressure granulite-facies metamorphism and subsequently cut, in greenschist facies, by minor (probably D_4) shear zones.

Based on microstructures and reaction relations between mineral phases, four mineral assemblages have been recognized from the high- and medium-pressure mafic granulites (mafic dykes): a prograde assemblage (M_1), a peak assemblage (M_2), pyroxene+plagioclase symplectite or corona (M_3), and hornblende+plagiocase symplectite (M_4) (O'Brien et al., 2005). The metamorphic evolution is characterized by a near-isothermal decompressional clockwise P-T path (Fig. 5).

The P-T conditions of the early prograde eclogite facies (M_1) cannot be quantitatively determined because of the absence of suitable minerals. Peak M_2 metamorphic mineral assemblages indicate conditions of 13.4–15.5 kbar and 770–840°C (Fig. 5). The high-pressure granulites may have undergone medium-pressure granulite-facies metamorphism following the high-pressure event, and the medium-pressure granulites may have resulted from retrograded high-pressure granulites (O'Brien et al., 2005). Medium to low-pressure granulite-facies conditions of 6.5–8.0 kbar and 750–830°C estimated for the M_3 mineral assemblage and core to rim compositional variations of the peak-M_2 minerals reflect a nearly isothermal decompression path. Such decompression paths require rapid unroofing of deep-seated metamorphic rocks relative to the rate of thermal relaxation and cooling. This can typically be accomplished by rapid erosional exhumation or extensional faulting (England and Richardson, 1977). P–T conditions of 4.5–6.0 kbar and 680–790°C estimated for the M_4 mineral assemblage indicate further decompression accompanied by cooling and retrogression and are represented by hydrous phase minerals in the mafic dykes. M_4 reflects exhumation to a still shallower crustal level.
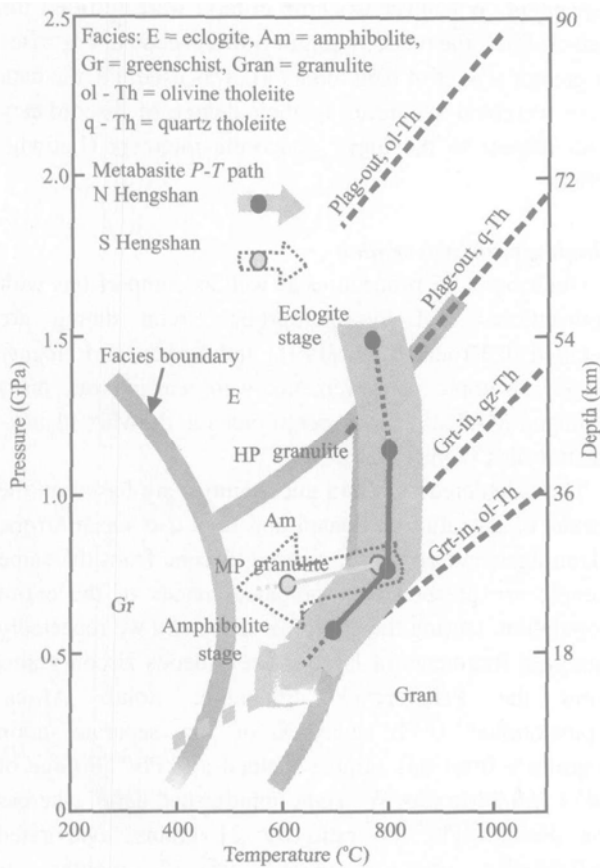
Fig. 5. Simplified *P-T* diagram adapted from O'Brien et al. (2005) and showing different metamorphic stages, recorded or inferred from microtextures, for the mafic granulite types in the Hengshan area. For detailed interpretation see O'Brien et al. (2005).

3 Previous Geochemistry and Geochronology

Li and Qian (1994) reported major and trace element data for the Hengshan granitoid gneisses and concluded that the moderately differentiated high-Al_2O_3 tonalite-trondhjemite-granodiorite assemblage is chemically akin to Archaean TTG-suites elsewhere in the world. REE patterns and the lack of a negative Eu-anomaly led these authors to conclude that the gneiss precursors were derived from melting of a mafic volcanic source, presumably in a subduction zone along an active continental margin. Gneisses of granitic composition were interpreted to be derived by partial melting of a presumably older TTG suite

Liu et al. (2002) demonstrated a remarkable similarity in the major and trace element chemistry of Hengshan and Fuping TTG gneisses with both units showing typical TTG features and plotting in the volcanic arc granitoid field on most discrimination diagrams. They concluded from this that the Hengshan and Fuping gneisses

originated as a single crustal block and remained as such during the early Proterozoic, a view supported by our data.

Published isotopic age data for rocks of the Hengshan complex are few and were summarized by Tian et al. (1992), Chang et al. (1994, 1999) Zhao et al. (2001a, b) and Kröner et al. (2005a). There are two Sm-Nd whole-rock isochron ages for mafic granulites (gabbroic dykes) of 2851±76 and 2818±86 Ma, respectively, interpreted as the emplacement ages for the mafic rocks (Tian et al., 1992). Multigrain U-Pb zircon analyses from a tonalitic gneiss N of the village of Yixingzhai (Yixingzhai granitoid gneisses in Fig. 2) provided discordant results with an upper concordia intercept age of 2520 Ma (interpreted as the protolith age) and a lower concordia intercept age of 1820 Ma (interpreted to reflect high-grade metamorphism) (Tian et al. (1992). Single zircons from this rock were further analyzed on SHRIMP and yielded an age of 2513±15 Ma (S.A. Wilde, reported in Kröner et al., 2002). As demonstrated below, the majority of gneisses in the Hengshan was emplaced between ~2500 and ~2520 Ma, and the mafic dykes are clearly intrusive into these gneisses. The above Sm-Nd ages are therefore suspect and much too old to represent the crystallization age of the dykes.

A 20-m wide, undeformed and seemingly unmetamorphosed dolerite dyke cutting all structures in the Hengshan gneisses and exposed in lower Big Stone Valley provided a U-Pb zircon age of 1769±2.5 Ma (Hall et al., 2002) which sets a lower limit to deformation, metamorphism and uplift in the Hengshan complex.

Kröner et al. (2002, 2005a) summarized new SHRIMP and evaporation zircon ages for the Hengshan, Wutai and Fuping complexes without providing analytical details and concluded from a comparative study that these three complexes define genetically related late Archaean to early Proterozoic igneous suites probably constituting a Japan-type magmatic arc.

4 Analytical Methods

Whole-rock geochemistry

Whole-rock sample powders were analyzed for major elements by ICP-AES in the Key Laboratory of Orogenic Belts and Crustal Evolution at Peking University. Details on the analytical procedure can be found in Xie et al. (1994) and Liu et al. (2004), and major element accuracy is within 0.1 weight per cent. Trace elements, including rare-earth elements (REE), were analyzed in the same laboratory in an Axiom multi-collector inductively coupled plasma mass spectrometer (MC-ICP-MS). Rock powders were accurately weighed (100 mg) into Savillex Teflon beakers, and a 5:3 mixture of $HF-HNO_3$ was added.

The beakers were capped and placed on a hot plate at 190° C until samples were completely digested. The samples were then diluted with 1% HNO_3 to a suitable concentration for analysis. Quantification was achieved using external standardization and standard addition. Standard Reference Materials SY-2 and MRG-1 were used to monitor the data quality during the course of this study. On the basis of duplicate analyses of international reference materials and samples, the precision and accuracy are estimated to be better than 2 % for all trace elements, except for U (9%).

SHRIMP II procedure

Zircons were handpicked and mounted in epoxy resin together with chips of the Perth Consortium standard CZ3. The mounts were then polished, cleaned and etched in 48% HF for about 20 seconds. Etching brings out the high -U, metamict parts of zircon. The etched zircons were photographed in reflected and transmitted light to bring out the internal structures, and the mount was then repolished.

Isotopic analyses were performed on the Perth Consortium SHRIMP II ion microprobe except for sample Ch 020903 which was analyzed in the Beijing Shrimp laboratory of the Chinese Academy of Geological Sciences. Both instruments are virtually identical, and their technical characteristics were outlined by De Laeter and Kennedy (1998). The analytical procedures are detailed in Claoué-Long et al. (1995) and Nelson (1997). The reduced $^{206}Pb/^{238}U$ ratios for CZ3 were normalized to 0.0914, which is equivalent to an age of 564 Ma. The error in the ratio $^{206}Pb*/U$ during analysis of all standard zircons during this study was between 1.33% and 1.65%. Analyses of samples and standards were alternated to allow assessment of Pb^+/U^+ discrimination. Sensitivity was around 23 cps/$\times 10^{-6}$/nA Pb. Raw data reduction followed the method described by Nelson (1997). Common Pb is considered to be surface-related (Kinny, 1986), and corrections have been applied using the ^{204}Pb-correction method and assuming the isotopic composition of Broken Hill lead (Cumming and Richards, 1975). The analytical data are presented in Table 1. Errors given on individual analyses are largely based on counting statistics and are at the 1-σ level and include the uncertainty of the standard added in quadrature. Stern (1997) provides a detailed account of the counting error assessment for SHRIMP analyses. Errors for pooled analyses are reported at the 2-σ level. The ages and 2σ errors of intercepts of the best-fit line with Concordia were calculated using the ISOPLOT program of Ludwig (1999). These errors were not multiplied with the square root of the MSWD since the absolute value of the intercept error is strongly model-dependent. Whenever isochron criteria were fulfilled for best-fit lines, the model 1 solution was accepted. For cases of greater scatter of data model 4U was used, i.e. the data were weighted according to their degree of discordancy with respect to the upper concordia intercept (Ludwig, 1994).

Single zircon evaporation

Our laboratory procedures as well as comparisons with conventional and ion-microprobe zircon dating are detailed in Kröner et al. (1991) and Kröner and Hegner (1998). Isotopic measurements were carried out on a Finnigan-MAT 261 mass spectrometer at the Max-Planck-Institut für Chemie in Mainz.

The calculated ages and uncertainties are based on the means of all ratios evaluated and their 2-σ mean errors. Mean ages and errors for several zircons from the same sample are presented as weighted means of the entire population. During the course of this study we repeatedly analyzed fragments of large, homogeneous zircon grains from the Palaborwa Carbonatite, South Africa. Conventional U-Pb analyses of six separate grain fragments from this sample yielded a $^{207}Pb/^{206}Pb$ age of 2052.2±0.8 Ma (2σ, W. Todt, unpublished data), whereas the mean $^{207}Pb/^{206}Pb$ ratio for 21 grains, evaporated individually over a period of 12 months, is 0.126634± 0.000026 (2σ error of the population), corresponding to an age of 2051.8 ±0.4 Ma, identical to the U-Pb age. The above error is considered the best estimate for the reproducibility of our evaporation data and corresponds approximately to the (mean) error reported for individual analyses in this study (Table 2). In the case of combined data sets the 2-σ mean error may become very low, and whenever this error was less than the reproducibility of the internal standard, we have used the latter value (that is, an assumed 2σ error of 0.000026).

The analytical data are presented in Table 2, and the $^{207}Pb/^{206}Pb$ spectra are shown in histograms that permit visual assessment of the data distribution from which the ages are derived. The evaporation technique provides only Pb isotopic ratios, and there is no *a priori* way to determine whether a measured $^{207}Pb/^{206}Pb$ ratio reflects a concordant age. Thus, all $^{207}Pb/^{206}Pb$ ages determined by this method are necessarily *minimum* ages. However, many studies have demonstrated that there is a very strong likelihood that these data represent true zircon crystallization ages when (1) the $^{207}Pb/^{206}Pb$ ratio does not change with increasing temperature of evaporation and/or (2) repeated analyses of grains from the same sample at high evaporation temperatures yield the same isotopic ratios within error. Comparative studies by evaporation, conventional U–Pb dating, and ion-microprobe analysis

Table 1 SHRIMP II analytical data for magmatic zircons from granitoid gneisses of the Hengshan Complex, China

Sample No.	U (×10⁻⁶)	Th (×10⁻⁶)	$^{206}Pb/^{204}Pb$	$^{208}Pb/^{206}Pb$	$^{207}Pb/^{206}Pb$	$^{206}Pb/^{238}U$	$^{207}Pb/^{235}U$	$^{206}Pb/^{238}U$ age±1σ	$^{207}Pb/^{235}U$ age±1σ	$^{207}Pb/^{206}Pb$ age±1σ
980809-1.1	325	298	6922	0.2604±14	0.1647±7	0.4729±79	10.74±19	2496±35	2501±17	2505±7
980809-2.1	403	242	39683	0.1696±8	0.1644±5	0.4478±82	10.15±19	2385±37	2449±18	2502±5
980809-3.1	1057	275	905	0.0926±26	0.1340±12	0.1364±25	2.52±54	825±14	1278±16	2152±16
980809-4.1	346	280	43605	0.2209±10	0.1642±5	0.4705±87	10.65±20	2486±38	2493±18	2499±5
980809-4.2	239	114	31845	0.1395±10	0.1646±6	0.4478±83	10.16±20	2385±37	2449±18	2503±7
980809-5.1	869	88	7009	0.0452±8	0.1333±5	0.2136±39	3.93±75	1248±21	1619±16	2142±7
980809-6.1	412	284	104932	0.1879±8	0.1641±5	0.4641±86	10.50±20	2457±38	2480±18	2498±5
980809-7.1	254	197	15162	0.2073±12	0.1646±6	0.4713±86	10.70±21	2489±38	2497±18	2504±6
980814-1.1	454	88	131199	0.0531±5	0.1621±5	0.4683±78	10.47±18	2476±34	2477±16	2478±5
980814-2.1	420	118	8921	0.0808±10	0.1624±6	0.4220±71	9.45±17	2269±32	2382±16	2480±7
980814-3.1	749	207	5742	0.0847±10	0.1621±6	0.3859±64	8.63±15	2104±30	2299±16	2478±6
980814-4.1	127	91	2464	0.1994±28	0.1626±13	0.4495±78	10.08±20	2393±35	2442±19	2483±14
980814-5.1	197	56	287935	0.0795±9	0.1625±8	0.4728±81	10.59±19	2496±35	2488±17	2482±8
990821-1	29	5	393700	0.0487±12	0.1671±15	0.4448±64	10.25±18	2372±28	2457±16	2529±15
990821-2	183	198	99900	0.3016±14	0.1670±6	0.4377±54	10.08±14	2341±24	2442±12	2528±6
990821-3	42	18	41841	0.1201±34	0.1665±18	0.4689±66	10.77±20	2479±29	2503±17	2523±18
990821-4	30	16	13033	0.1455±32	0.1656±18	0.4817±69	10.99±21	2534±30	2523±18	2513±18
990821-5	44	23	127065	0.1547±21	0.1663±13	0.4510±61	10.34±17	2400±27	2466±15	2521±13
990821-6	77	37	52301	0.1341±13	0.1668±9	0.4675±61	10.75±16	2472±27	2502±14	2526±9
990838-1	145	102	613497	0.2010±13	0.1848±8	0.4532±57	11.55±16	2409±25	2569±13	2697±7
990838-2	43	29	22707	0.1914±30	0.1851±16	0.4832±68	12.33±22	2541±30	2630±16	2699±15
990838-3	222	116	34376	0.1443±9	0.1853±6	0.4814±60	12.30±16	2533±26	2628±12	2701±5
990838-4	253	184	16644	0.2107±10	0.1857±6	0.4620±57	11.83±16	2448±25	2591±12	2705±5
990838-5	189	87	26330	0.1304±10	0.1842±7	0.4777±60	12.13±16	2517±26	2615±13	2691±6
990838-6	296	163	186220	0.1494±7	0.1857±5	0.4767±58	12.21±16	2513±26	2620±12	2705±4

(continued 1)

Sample No.	U (×10⁻⁶)	Th (×10⁻⁶)	206Pb/204Pb	208Pb/206Pb	207Pb/206Pb	206Pb/238U	207Pb/235U	206Pb/238U age±1σ	207Pb/235U age±1σ	207Pb/206Pb age±1σ
990843-1	127	60	12185	0.1287±13	0.1866±9	0.5254±111	13.52±30	2722±47	2717±21	2712±8
990843-2	87	40	6882	0.1285±20	0.1866±12	0.5021±107	12.92±30	2623±46	2674±22	2712±11
990843-3	54	26	5445	0.1397±26	0.1862±16	0.5063±110	13.99±31	2641±47	2680±23	2709±14
990843-4	152	85	6684	0.1536±13	0.1866±9	0.5185±109	13.34±30	2693±46	2704±21	2712±8
990843-5	83	25	6761	0.0842±19	0.1867±13	0.5094±109	13.11±30	2654±47	2688±22	2713±11
990843-6	102	67	15642	0.1856±16	0.1862±10	0.4715±100	12.10±27	2490±44	2613±21	2709±9
990847-1	256	40	9798	0.0736±8	0.1642±7	0.3162±66	7.16±16	1771±32	2132±19	2500±7
990847-2	81	30	14364	0.1094±18	0.1664±12	0.4549±97	10.43±24	2417±43	2474±22	2521±12
990847-3	176	67	7251	0.1040±12	0.1670±8	0.4661±98	10.73±24	2466±43	2500±21	2528±8
990847-4	50	23	3671	0.1177±30	0.1672±17	0.4812±105	11.09±28	2532±46	2531±24	2530±17
990847-5	166	47	2077	0.0959±20	0.1661±11	0.4019±84	9.20±21	2178±39	2358±21	2518±11
990859-1	147	56	77622	0.1410±14	0.1461±8	0.3876±48	7.81±11	2112±22	2209±13	2301±9
990859-2	298	316	131234	0.2983±11	0.1651±5	0.4701±58	10.70±14	2484±25	2497±12	2508±5
990859-3	260	332	56054	0.3534±12	0.1646±5	0.4690±58	10.65±14	2479±25	2493±12	2504±5
990859-4	408	564	95785	0.3931±11	0.1648±4	0.4546±55	10.33±13	2415±25	2465±12	2505±4
990873-1	73	62	101010	0.2552±22	0.1641±10	0.4409±57	9.98±15	2355±26	2433±14	2498±11
990873-2	76	54	392157	0.1978±16	0.1639±9	0.4427±57	10.00±15	2363±25	2435±14	2496±9
990873-3.1	124	99	44014	0.2223±13	0.1645±7	0.4706±59	10.68±15	2486±26	2495±13	2503±7
990873-3.2	1009	99	5896	0.0407±4	0.1632±3	0.3106±37	6.99±9	1744±18	2110±11	2489±3
990873-4	53	54	236967	0.2900±23	0.1638±11	0.4727±62	10.67±16	2495±27	2495±14	2495±11
020903-1	330	251	2318	0.2233±21	0.1568±10	0.4239±38	9.16±11	2278±17	2355±11	2422±11
020903-2	370	230	12945	0.1699±19	0.1567±11	0.2878±25	6.22±7	1631±12	2007±10	2420±12
020903-3	549	219	1213	0.1460±22	0.1567±11	0.2934±25	6.34±7	1659±12	2024±10	2421±12
020903-4	266	138	6343	0.1358±27	0.1562±13	0.3963±36	8.54±11	2152±17	2290±12	2415±15
020903-5	504	449	5445	0.2364±39	0.1563±19	0.2294±20	4.95±8	1331±10	1810±13	2416±20

Sample Ch 020903 data are from Beijing laboratory.

(continued 2)

Sample No.	U ($\times10^{-6}$)	Th ($\times10^{-6}$)	$^{206}Pb/^{204}Pb$	$^{208}Pb/^{206}Pb$	$^{207}Pb/^{206}Pb$	$^{206}Pb/^{238}U$	$^{207}Pb/^{235}U$	$^{206}Pb/^{238}U$ age$\pm1\sigma$	$^{207}Pb/^{235}U$ age$\pm1\sigma$	$^{208}Pb/^{206}Pb$ age$\pm1\sigma$
HG4-1	2912	251	1783	0.0343±7	0.1472±4	0.3034±77	6.16±16	1708±38	1999±23	2314±4
HG4-2	431	147	6163	0.0916±11	0.1602±6	0.4604±118	10.17±27	2441±52	2451±24	2458±6
HG4-3	746	185	2740	0.0555±9	0.1481±5	0.5396±138	11.02±29	2782±58	2525±24	2324±6
HG4-4	1881	388	1479	0.0573±10	0.1438±5	0.3809±97	7.55±20	2080±45	2179±23	2273±6
HG4-5	1485	344	1233	0.1646±13	0.1472±6	0.3383±86	6.87±18	1878±41	2094±23	2314±7
HG4-6	2190	310	1381	0.1461±10	0.1426±5	0.3373±86	6.63±17	1874±41	2064±23	2260±6
HG4-7	238	37	1071	0.1337±31	0.1322±14	0.4084±106	7.44±22	2208±49	2166±26	2127±18
HG4-8	747	55	5025	0.1087±9	0.1494±5	0.3935±101	8.11±21	2139±46	2243±24	2339±6
HG4-9	133	57	2123	0.0981±26	0.1525±13	0.6844±181	14.39±41	3361±69	2776±27	2374±15
HG4-10	1045	118	19608	0.0448±9	0.1525±5	0.4756±121	10.00±26	2508±53	2435±24	2374±5
HG4-11	589	99	7407	0.0464±7	0.1519±5	0.4660±119	9.76±26	2466±52	2412±24	2367±5
HG4-12	581	83	2809	0.0429±11	0.1504±6	0.4110±105	8.52±22	2219±48	2288±24	2350±7
HG5-1	34	0.4	7840	0.012940	0.1164±25	0.3233±62	5.19±16	1806±30	1850±25	1901±38
HG5-2	138	79	16287	0.1614±16	0.1649±10	0.4512±76	10.26±19	2401±34	2459±17	2507±10
HG5-3	67	28	3202	0.1209±33	0.1622±19	0.4281±77	9.58±22	2297±35	2395±21	2479±20
HG5-4	141	71	7686	0.1433±17	0.1648±11	0.4636±79	10.53±20	2455±35	2483±18	2506±11
HG5-5	109	51	7648	0.1324±22	0.1682±13	0.4708±82	10.92±22	2487±36	2516±18	2540±13
HG5-6	458	339	35410	0.1976±9	0.1664±6	0.4668±78	10.94±19	2513±34	2518±16	2522±6
HG5-7	166	2.7	18513	0.0096±16	0.1172±11	0.3498±59	5.65±11	1934±28	1924±17	1914±17
HG5-8	194	139	9759	0.1962±18	0.1658±10	0.4728±80	10.81±20	2496±35	2507±17	2516±10
HG5-9	116	66	4255	0.1550±25	0.1683±14	0.4750±82	11.02±22	2505±36	2525±19	2541±14
HG5-10	177	122	12189	0.1962±16	0.1671±10	0.4946±83	11.39±21	2590±36	2556±17	2529±10
HG5-11	82	0.1	7335	0.0067±61	0.1170±30	0.3541±64	5.71±19	1954±30	1933±28	1911±45
HG5-12	129	81	12396	0.1710±22	0.1677±13	0.4842±83	11.20±22	2545±36	2540±18	2535±13
HG5-13	39	0.6	3581	0.0189±93	0.1175±45	0.3467±69	5.62±25	1919±33	1918±38	1918±68
HG5-14	54	19	3318	0.1033±50	0.1641±28	0.4401±84	9.96±27	2351±37	2431±25	2498±28
HG5-15	33	13	1673	0.1092±79	0.1681±41	0.4662±97	10.80±37	2467±42	2506±31	2539±40
HG6-1	42	20	2874	0.1371±51	0.1667±27	0.5067±98	11.65±31	2643±42	2576±25	2525±27
HG6-2	27	14	73115	0.1582±41	0.1700±28	0.4745±101	11.12±32	2503±44	2534±26	2558±27
HG6-3	122	46	6331	0.1154±41	0.1647±22	0.3714±65	8.43±20	2036±30	2279±21	2505±22
HG6-4	26	13	3696	0.1571±71	0.1656±37	0.4830±101	11.03±36	2540±44	2525±30	2513±37

(continued 3)

Sample No.	U (×10⁻⁶)	Th (×10⁻⁶)	$^{206}Pb/^{204}Pb$	$^{208}Pb/^{206}Pb$	$^{207}Pb/^{206}Pb$	$^{206}Pb/^{238}U$	$^{207}Pb/^{235}U$	$^{206}Pb/^{238}U$ age±1σ	$^{207}Pb/^{235}U$ age±1σ	$^{207}Pb/^{206}Pb$ age±1σ
HG6-5	54	23	5409	0.1255±43	0.1704±24	0.4679±87	10.99±27	2474±38	2522±23	2561±23
HG6-6	86	38	14959	0.1248±24	0.1664±15	0.4824±85	11.07±23	2538±37	2529±19	2522±15
HG6-7	129	80	5970	0.1745±21	0.1673±12	0.4580±79	10.56±21	2431±35	2486±18	2531±12
HG6-8	40	26	4037	0.1810±47	0.1700±25	0.4636±89	10.86±28	2455±39	1512±24	1557±25
HG6-9	49	12	3465	0.0708±58	0.1689±31	0.4966±98	11.56±33	2599±42	2570±26	2546±31
HG6-10	34	21	1387	0.1704±179	0.1671±83	0.4437±100	10.22±58	2367±45	2455±52	2529±83
HG6-11	253	209	11150	0.2197±22	0.1666±12	0.4333±73	9.95±19	2321±33	2430±18	2524±12
HG6-12	91	59	9532	0.1962±23	0.1646±14	0.4478±78	10.16±21	2386±35	2450±19	2503±14
HG7-1	205	100	1038	0.1374±29	0.1656±15	0.4371±64	9.98±18	2338±29	2433±17	2514±15
HG7-2	102	23	4432	0.0591±20	0.1654±14	0.5040±78	11.49±21	2631±33	2564±17	2512±14
HG7-3	85	19	828	0.0750±54	0.1632±27	0.4834±77	10.88±26	2542±33	2513±22	2489±28
HG7-4	65	21	1860	0.0816±44	0.1638±24	0.4754±78	10.74±25	2507±34	2500±21	2495±24
HG7-5	71	45	2566	0.1741±41	0.1658±22	0.4725±77	10.80±24	2495±33	2506±20	2516±22
HG7-6	61	45	1567	0.2046±55	0.1645±27	0.4729±80	10.72±27	2496±35	2499±23	2502±28
HG7-7	712	204	2049	0.0138±48	0.1644±26	0.538±168	12.20±45	2777±70	2620±34	2501±27
HG7-8	49	14	4689	0.0927±35	0.1638±23	0.3810±67	8.60±20	2081±31	2297±21	2495±24
HG7-9	59	30	2653	0.1439±59	0.1654±30	0.4409±74	10.06±26	2355±33	2440±24	2512±30
HG7-10	64	59	920	0.2547±76	0.1650±36	0.4826±83	10.98±32	2538±36	2521±27	2508±36
HG7-11	95	53	2941	0.1597±31	0.1655±17	0.4701±74	10.73±21	2484±32	2500±18	2513±17
HG7-12	199	5.9	3034	0.0095±22	0.1401±13	0.3909±57	7.55±14	2127±27	2179±16	2228±16
HG7-13	49	42	1579	0.2237±67	0.1642±32	0.4567±77	10.34±28	2425±34	2465±25	2499±33
HG7-14	49	39	2281	0.2224±53	0.1650±26	0.4893±84	11.13±28	2568±36	2534±23	2507±27
HG7-15	78	95	4056	0.3377±38	0.1656±18	0.4681±74	10.69±22	2475±33	2497±19	2514±18
HG7-16	66	53	3097	0.2390±46	0.1636±23	0.4791±78	10.80±24	2523±34	2506±21	2493±23
HG7-17	36	16	3478	0.1040±70	0.1644±36	0.6758±121	15.32±46	3328±47	2835±28	2501±36
HG7-18	86	69	1833	0.2124±38	0.1652±19	0.4755±75	10.83±23	2507±33	2508±19	2509±20
HG7-19	68	68	2810	0.2758±43	0.1649±21	0.4764±77	10.83±24	2512±34	2509±20	2506±21
HG7-20	69	38	3837	0.1543±34	0.1652±19	0.4760±77	10.84±23	2510±34	2510±20	2510±20

Table 2 Zircon morphology and isotopic data from single grain evaporation

Sample No.	Zircon colour and morphology	Grain#	Mass scans[1]	Evaporation temp (°C)	Mean $^{207}Pb/^{206}Pb$ ratio[2] and 2-σm error	$^{207}Pb/^{206}Pb$ age and 2-σm error
Ch 980802	Light grey to light yellow-brown, long-prismatic, ends rounded	1	55	1607	0.164329±72	2500.7±0.7
		2	99	1602	0.164328±51	2500.7±0.5
		3	88	1599	0.164286±52	2500.3±0.5
Mean of 3	**Grains**	1–3	242		0.164313±32	**2500.5±0.3**
Ch 980809	Dark red-brown, yellow-brown, long-prismatic, ends rounded	1	88	1604	0.164578±59	2503.2±0.6
		2	143	1607	0.164597±39	2503.4±0.4
		3	121	1602	0.164627±55	2503.7±0.6
Mean of 3	**Grains**	1–3	352		0.164603±28	**2503.5±0.3**
Ch 980811	Light yellow to long-prismatic, idiomorphic rounded ends	1	88	1603	0.184916±57	2697.5±0.5
		2	132	1607	0.184854±44	2696.9±0.4
		3	110	1604	0.184887±43	2697.2±0.4
		4	165	1602	0.184866±33	2697.0±0.3
Mean of 4	**Grains**	1–4	495		0.184876±21	***2697.1±0.3**
Ch 989814	Light grey, long-prismatic, ends rounded	1	132	1607	0.162145±33	2478.2±0.3
		2	110	1603	0.162129±49	2478.0±0.5
		3	77	1603	0.162159±59	2478.3±0.6
		4	132	1601	0.162138±35	2478.1±0.4
		5	121	1600	0.162108±49	2477.8±0.5
		6	77	1604	0.162165±53	2478.4±0.6
Mean of 6	**Grains**	1–6	649		0.162149±18	***2478.2±0.3**
Ch 980824	Yellow-brown, long-prismatic, ends rounded.	1	77	1599	0.181928±65	2670.5±0.6
		2	88	1600	0.181942±49	2670.7±0.4
Mean of 2	**Grains**	1, 2	165		0.181936±40	**2670.6±0.4**
Ch 980833	Light yellow-brown, long-prismatic, ends slightly rounded	1	88	1605	0.163533±69	2492.5±0.7
		2	88	1607	0.163498±47	2492.2±0.5
		3	110	1605	0.163520±42	2492.4±0.4
		4	132	1607	0.163541±30	2492.6±0.3
Mean of 4	**Grains**	1–4	418		0.163525±23	***2492.4±0.3**
Ch 980838	Light grey-brown long-prismatic, ends rounded	1	55	1602	0.164556±71	2503.0±0.7
		2	120	1598	0.164561±56	2503.1±0.6
		3	104	1603	0.164581±43	2503.3±0.5
		4	99	1599	0.164511±46	2502.6±0.5
		5	82	1599	0.164553±53	2503.0±0.5
		6	82	1600	0.164536±33	2502.8±0.3
Mean of 6	**Grains**	1–6	542		0.164550±21	***2503.0±0.3**
Ch 980857	Dark red-brown, long-prismatic, ends rounded	1	110	1601	0.161438±45	2470.8±0.5
		2	75	1598	0.161419±58	2470.6±0.6
		3	80	1603	0.161447±56	2470.9±0.6
		4	77	1604	0.161372±50	2470.1±0.5
		5	93	1599	0.161356±38	2469.8±0.4
Mean of 5	**Grains**	1–5	435		0.161407±22	***2470.5±0.3**
Ch 990843	Light yellow-brown, long-prismatic, rounded terminations	1	104	1597	0.186486±91	2711.4±0.8
		2	122	1599	0.186407±64	2710.7±0.6
		3	109	1598	0.186436±49	2711.0±0.4
		4	105	1598	0.186472±29	2711.3±0.3
Mean of 4	**Grains**	1–4	440		0.186450±30	**2711.1±0.3**
Ch 990847	Clear to ligh yellow-brown, long-prismatic, ends well rounded.	1	105	1598	0.166422±54	2522.0±0.5
		2	130	1599	0.166394±62	2521.7±0.6
		3	125	1599	0.166363±61	2521.4±0.6
Mean of 3	**Grains**	1–3	360		0.166391±35	**2521.7±0.4**
Ch 990854	Pink to light grey, long-prismatic, ends rounded	1	119	1600	0.164656±61	2504.0±0.6
		2	76	1599	0.164626±63	2503.7±0.6
		3	79	1601	0.164763±72	2505.1±0.7
		4	83	1599	0.164799±62	2505.5±0.6
Mean of 4	**Grains**	1–4	357		0.164706±33	**2504.6±0.3**

(continued)

Sample No.	Zircon colour and morphology	Grain No.	Mass scans[1]	Evaporation temp (°C)	Mean $^{207}Pb/^{206}Pb$ ratio[2] and 2-σm error	$^{207}Pb/^{206}Pb$ age and 2-σm error
Ch 990859	Pink to light grey, long-prismatic, ends rounded	1	80	1600	0.164727±51	2504.8±0.6
		2	73	1599	0.164741±62	2504.9±0.6
		3	102	1601	0.164684±45	2504.3±0.5
		4	78	1599	0.164713±58	2504.6±0.6
Mean of 4	Grains	1–4	333		0.164714±29	**2504.6±0.3**
Ch 990871	Clear to pinkt and light grey, long-prismatic, ends rounded	1	111	1602	0.164472±55	2502.2±0.6
		2	63	1599	0.164459±65	2502.0±0.7
		3	114	1598	0.164514±57	2502.6±0.6
		4	88	1600	0.164450±60	2501.9±0.6
		5	82	1599	0.164502±72	2502.5±0.8
Mean of 5	Grains	1–5	458		0.164482±28	**2502.3±0.3**
Ch 990881	Pink to red, long-prismatic, idiomorphic, ends little rd.	1	85	1599	0.141750±73	2248.7±0.9
		2	72	1599	0.141741±96	2248.6±1.2
		3	86	1601	0.141718±56	2248.3±0.7
Mean of 3	Grains	1–3	243		0.141736±43	**2248.5±0.5**

[1] Number of $^{207}Pb/^{206}Pb$ ratios evaluated for age assessment; [2] observed mean ratio corrected for non-radiogenic Pb where necessary. Errors based on uncertainties in counting statistics. *Errors of combined mean ages (bold print) are based on reproducibility of internal standard at 0.000027 (2σ).
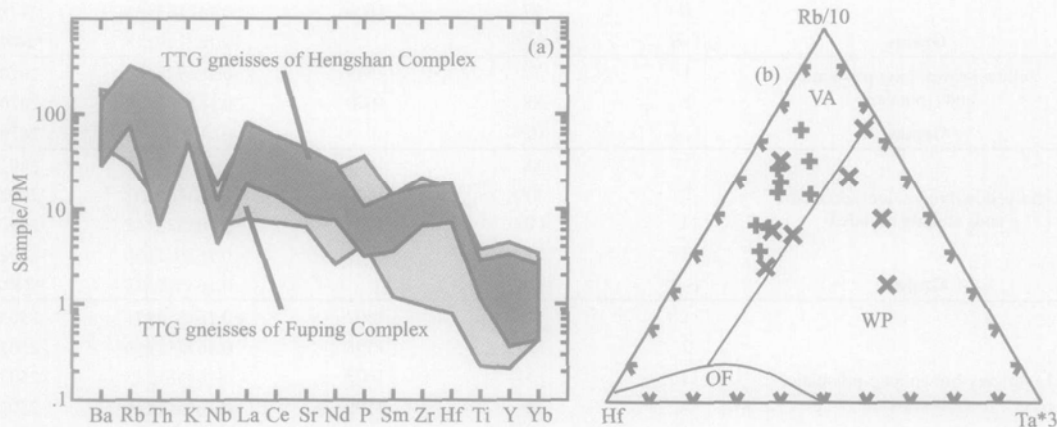
Fig. 6. (a) Primitive mantle-normalized multielement diagram of granitoid gneisses from the Hengshan (dark grey) and Fuping (light grey) Complexes, based on data of Table 1 and Liu et al. (2004). (b) Triangular Rb-Hf-Ta-plot (Harris et al., 1986) showing samples of Hengshan (+) and Fuping (x) TTG gneisses. Designated fields are: VA − Volcanic arc; OF − Ocean floor; WP − Within-plate. Data from Table 1 and Liu et al. (2004).

have shown this to be correct (Kröner et al., 1991, 1999; Cocherie et al., 1992; Jaeckel et al., 1997; Karabinos, 1997).

5 Whole-rock Geochemistry

Geochemically, the Hengshan grey gneisses are similar to Archaean TTG-suites elsewhere is the world (e.g. Martin, 1987) that have been interpreted as root zones of arc complexes (e.g. Cassidy et al., 1991; Percival, 1994). Our analytical data for whole-rock splits from some of the same samples from which zircons were separated are given in Table 3. These rocks are metaluminous to peraluminous, define a calc-alkaline trend, as already noted by Li and Qian (1994) and Liu et al. (2002), and are

characterized by a wide range in SiO_2, high Na_2O, Ba, Sr and low Y. REE-patterns are similar to the Fuping TTG-assemblage (Liu et al., 2002) and Archaean granitoids elsewhere in the world, and only the most differentiated granodiorites and granites exhibit slight negative Eu-anomalies. Selective enrichment in LIL-elements and marked depletion in Nb, Ta and Ti are probably derived from magmatic precursors with a strong mantle signature, modified by a subduction component and variable contributions from older crust (Pearce et al., 1984; Harris et al., 1986). A particularly diagnostic discriminant for the tectonic setting is the Rb-Hf-Ta triangular plot for felsic to intermediate magmatic rocks in which arc-derived suites occupy a field distinct from rocks generated in within-plate and ocean floor settings (Harris et al., 1986).

Table 3 Chemical composition of selected granitoid gneisses from the Hengshan Complex, North China Craton (major elements in weight%, trace elements in ppm)

Sample No.	980802	980803	980804	980806	980811	980814	980824	980825	980833	980838
SiO_2	65.89	67.90	52.70	66.75	68.15	60.21	71.93	68.53	69.34	64.12
TiO_2	0.64	0.46	1.86	0.43	0.42	0.52	0.34	0.50	0.25	0.30
Al_2O_3	13.81	15.27	12.98	15.63	15.84	16.89	14.66	15.61	17.01	18.17
FeO	4.13	2.58	10.23	2.26	2.46	4.06	1.54	2.23	1.34	1.83
Fe_2O_3	1.57	1.38	4.13	1.16	0.83	1.60	0.81	1.10	0.29	1.02
MnO	0.07	0.05	0.19	0.04	0.03	0.08	0.02	0.05	0.01	0.05
MgO	3.23	1.52	3.47	1.77	1.74	3.33	0.55	1.29	0.65	1.84
CaO	2.96	2.93	6.43	4.28	2.62	4.72	1.95	3.37	3.30	5.22
Na_2O	2.47	4.11	2.48	4.62	4.59	5.03	3.73	4.46	5.27	4.35
K_2O	3.30	1.85	2.33	1.48	1.95	1.75	3.86	1.58	1.57	1.97
P_2O_5	0.15	0.09	0.46	0.14	0.13	0.23	0.08	0.14	0.07	0.16
LOI	1.50	1.64	1.88	1.22	0.90	1.34	0.66	1.10	1.03	1.06
Total	99.72	99.78	99.74	99.78	99.66	99.76	100.13	99.96	100.13	100.09
Cr	201	168	157	189	124	156	206	218	99	139
Co	25.8	12.6	54.8	13.0	10.4	18.2	7.85	10.7	6.99	11.5
Ni	51.9	22.6	44.7	28.8	15.9	35.8	12.3	13.8	13.4	22.2
Cu	86.4	36.8	88.4	26.6	18.2	8.69	10.9	14.4	8.82	34.2
Zn	76.4	83.4	222	84.9	83.6	87.4	147	88.5	43.0	55.6
Rb	126	69.8	59.1	48.9	80.0	52.9	197	51.8	46.2	68.6
Sr	175	366	297	529	290	682	385	312	904	646
Y	7.74	7.14	35.2	7.06	5.42	15.0	7.29	3.66	1.64	4.83
Zr	136	121	230	142	148	196	188	136	73.3	134
Nb	8.23	6.23	14.0	6.64	4.44	8.07	8.53	5.41	3.06	7.38
Sn	1.77	0.95	2.05	1.01	0.78	1.55	2.03	0.71	0.44	0.78
Cs	1.99	2.36	1.96	1.29	1.42	1.23	4.46	5.51	1.63	4.20
Ba	701	424	698	508	201	625	956	388	545	548
La	43.2	13.2	34.0	13.6	12.1	55.1	42.3	14.9	14.7	20.2
Ce	81.8	28.5	80.0	31.0	24.3	105	80.4	30.5	26.9	43.1
Pr	9.12	3.21	9.62	3.62	2.68	11.1	8.25	3.24	2.84	5.08
Nd	33.0	13.1	42.1	16.5	10.2	41.1	28.2	13.1	10.7	19.7
Sm	4.62	2.32	9.17	3.23	1.97	6.35	4.09	1.90	1.55	3.02
Eu	1.18	0.72	2.28	0.89	0.55	1.58	1.02	0.63	0.87	0.91
Gd	4.17	2.15	9.13	2.51	1.95	6.50	3.82	1.74	1.42	2.62
Tb	0.44	0.29	1.23	0.29	0.25	0.70	0.37	0.18	0.10	0.24
Dy	1.75	1.21	7.03	1.29	1.08	3.08	1.51	0.86	0.39	0.99
Ho	0.31	0.29	1.33	0.29	0.27	0.63	0.31	0.17	0.08	0.17
Er	0.80	0.80	3.74	0.74	0.61	1.48	0.84	0.32	0.60	0.48
Tm	0.10	0.12	0.55	0.08	0.08	0.19	0.08	0.03	0.02	0.06
Yb	0.65	0.69-	3.34	0.64	0.46	1.30	0.55	0.23	0.21	0.42
Lu	0.12	0.12	0.53	0.10	0.06	0.19	0.08	0.04	0.02	0.07
Hf	4.09	3.18	6.03	4.35	4.11	5.78	5.07	4.38	2.17	3.98
Ta	0.92	0.80	0.90	0.38	0.48	0.66	0.75	0.52	0.20	0.46
Pb	8.95	5.26	9.88	8.96	5.40	11.10	18.75	3.71	16.63	8.91
Bi	0.14	0.06	0.16	0.05	0.03	0.04	0.02	0.14	0.02	0.17
Th	20.6	3.17	4.27	1.12	4.04	12.0	13.9	1.48	0.57	4.95
U	1.14	0.57	0.87	0.26	0.53	0.28	1.51	0.23	0.17	1.20

Table 4 Summary of emplacement ages for granitoid orthogneisses from Hengshan, northern Shaanxi Province, China[1]

No. in Fig. 2	Sample No.	Rock type and description	Zircon age (Ma)	Dating method[2]
		Age group 2712-2670 Ma		
15	990843	Grey trondhjemitic gneiss, from migmatite domain, GWV	2712±2	SHRIMP
	Same sample		2711.1±0.3	Evap.
14	990838	Well foliated grey biotite gneiss, BSV	2701±5.5	SHRIMP
5	980811	Grey granodioritic gneiss, GWV	2697.1±0.3	Evap.
7	980824	Finely layered, fine-grained biotite gneiss (felsic metavolcanic?), GWV	2670.6±0.4	Evap.
13	990821	Finely layered, fine-grained biotite gneiss (felsic metavolcanic?), BSV	2526±4.7	SHRIMP
27	HG 5	Garnetiferous trondhjemitic gneiss, roadcut near Yanmenguan	2520±10	SHRIMP
		Two euhedral grains from same sample	1912±9	SHRIMP
18	990847	Grey, unveined trondhjemitic gneiss from migmatitic sequence, BSV	2524±8	SHRIMP
	Same sample		2521.7±0.4	Evap
28	HG 6	Trondhjemitic gneiss, roadcut near Yanmenguan	2526±12	SHRIMP
21	990859	Dioritic gneiss from margin of metagabbro boudin, LSV	2506±5	SHRIMP
	Same sample		2504.6±0.3	Evap.
20	990854	Trondhjemitic gneiss in sheared contact with metagabbro boudin, LSV	2504.6±0.3	Evap.
17	990845	Coarse-grained, well foliated tonalitic gneiss, BSV	2504.4±0.4	Evap.
10	980838	Trondhjemitic gneiss near foliated metagabbro boudin, Ruyue Valley	2503.0±0.3	Evap.
4	980809	Coarse grained, foliated pegmatitic red granite-gneiss, BSV	2501±3	SHRIMP
	Same sample		2503.5±0.3	Evap.
2	980803	Homogeneous felsic gneiss (highly sheared granite), BSV	2502.3±0.6	Evap.
22	990871	Tonalitic gneiss, small side valley of Ruyue Valley	2502.3±0.3	Evap.
29	HG 7	Trondhjemitic gneiss, roadcut near Yanmenguan	2507±4	SHRIMP
1	980802	Homogeneous tonalitic gneiss, not compositionally layered, BSV	2500.5±0.3	Evap.
23	990873	Well foliated granite gneiss from migmatitic assemblage, SW of Guaner	2499±6	SHRIMP
	Same sample	.	2497.6±0.3	Evap
11	980845	Foliated, slightly sheared trondhjemitic gneiss, LSV	2498.8±0.3	Evap.
8	980825	Fine-grained, highly strained granite-gneiss, LSV	2496.3±0.3	Evap.
9	980833	Granitic gneiss, LSV	2492.4±0.3	Evap.
6	980814	Dioritic gneiss at outer margin of gabbroic boudin, GWV	2479±3	SHRIMP
	Same sample		2478.2±0.3	Evap.
12	990803	Dioritic gneiss with melt patches, BSV	2455±2	SHRIMP
		one euhedral zircon grain from melt patch of same sample	1881±8	SHRIMP
25	020903	Red migmatitic gneiss, LSV	2420±3	SHRIMP
		Age group 2359-2112 Ma		
3	980806	Fine-grained granitic orthogneiss, BSV	2358.7±0.5	Evap.
19	990850	Layered trondhjemitic gneiss, BSV	2329.7±0.6	Evap.
26	HG 4	Pegmatitic granite-gneiss, BSV	2331±36	SHRIMP
24	990881	Pegmatite cutting older gneisses in LSV	2248.5±0.5	Evap.
16	990844	Red anatectic granite from migmatitic assemblage, GWV	2113±8	SHRIMP
	Same sample		2112.3±0.6	Evap.

[1] Analytical data in Tables 3 and 4; [2] SHRIMP – U/Pb age with 2-σ error, based on SHRIMP II analysis (Table 3). Evap. – Single grain evaporation ^{207}Pb/^{206}Pb age with 2-σ(mean) error, see Table 4. BSV – Big Stone Valley; LSV – Little Stone Valley; GWV – Great Wall Valley.
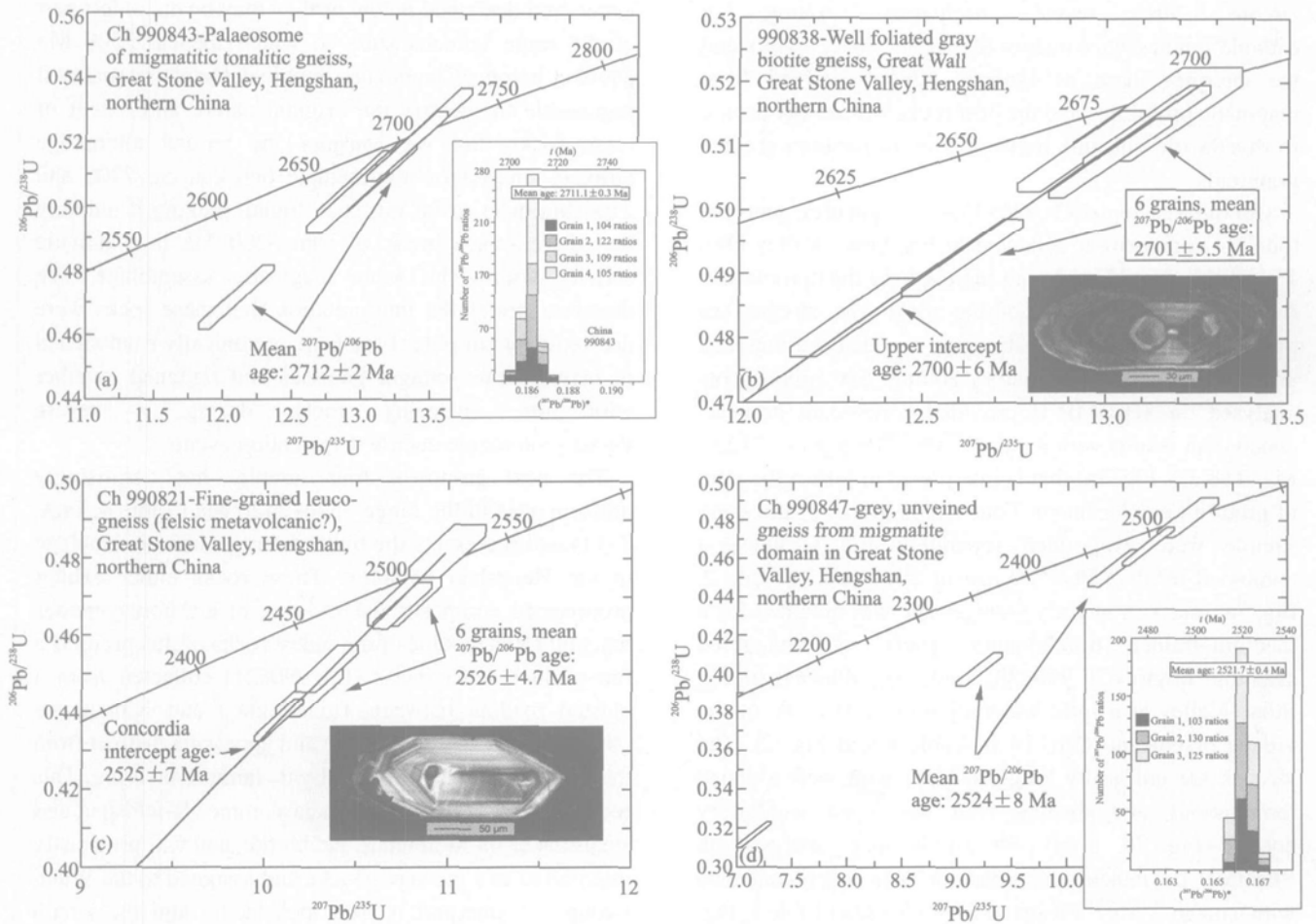
Fig. 7. Concordia diagrams showing SHRIMP analyses of zircons from Hengshan granitoid gneisses. Data boxes for each analysis are defined by standard errors in $^{207}Pb/^{235}U$, $^{206}Pb/^{238}U$ and $^{207}Pb/^{206}Pb$. (a) Palaeosome of migmatitic gneiss sample Ch 980843. Inset shows histogram with distribution of radiogenic Pb isotope ratios derived from evaporation of 4 single zircons from same sample, integrated from 440 ratios. (b) Grey biotite gneiss sample Ch 980838; inset shows CL-image with good oszillatory zoning; (c) Fine-grained leucocratic gneiss sample Ch 990821 (felsic metavolcanic rock?); inset shows euhedral magmatic grain with excellent oszillatory zoning (d) Palaeosome from migmatitic gneiss sample Ch 990847. Inset shows histogram with distribution of radiogenic Pb isotope ratios derived from evaporation of 3 single zircons from same sample, integrated from 360 ratios.

Fig. 6b shows such a plot for Hengshan gneisses dated by us which clearly supports their arc derivation. There are also chemical similarities with the Jurassic Bonanza arc on Vancouver Island, Canada (DeBari et al., 1999), the Talkeetna arc of southern Alaska (DeBari and Sleep, 1991), the Cretaceous Ryoke arc-granitoids of southwestern Japan (Kutsukake, 2002) and the Archaean Pikwitonei gneisses in Canada (Percival, 1994). The granitoids of the Neoproterozoic Goiás magmatic arc of Brazil (Viana et al., 1995) serve as another example.

6 Zircon Ages for the Hengshan Complex and Interpretation

Single zircon ages were obtained from granitoid gneisses of the Hengshan complex using SHRIMP II and the evaporation technique, and the ages are summarized in

Table 4, whereas the analytical data are presented in Tables 1 and 2. Our samples mainly come from the valleys in the central Hengshan, but also from roadcuts near Yanmenguan, and locations are shown in Fig. 2, with numbers corresponding to those in Table 4.

The oldest rocks in the Hengshan complex are light to medium grey gneisses of tonalitic to granitic composition, predominantly medium-grained, that occur interlayered in the younger granitoid gneisses but which are difficult to recognize as separate units in the field. Some of these rocks have previously been interpreted as paragneisses, possibly derived from greywacke-type protoliths (Li and Qian, 1994; Tian et al., 1996), but the zircons are uniformly thin and long-prismatic, with slight rounding at their terminations due to metamorphic corrosion (e.g. Fig. 7b, inset) that is typical for rocks in high-grade terrains (Kröner et al., 1994; Hoskin and Black, 2000). Most

zircons also reveal oscillatory zoning in cathodoluminescence images (e.g., Figs. 7b, c, insets), and we interpret these as igneous zircons derived from magmatic protoliths, and the host rocks were either dacitic to rhyodacitic volcanic rocks or fine- to medium-grained granitoids.

Our oldest sample (Ch 990843) is a migmatitic gneiss of tonalitic composition collected in Big Stone Valley (No. 15 in Table 4 and Fig. 2) and representing the hornblende-rich palaeosome portion of the rock. The zircons are predominantly long-prismatic with rounded terminations and well developed oscillatory zoning. Six zircon spots analysed on SHRIMP II provided concordant or near-concordant results with a mean ^{207}Pb/^{206}Pb age of 2712±2 Ma (Table 1, Fig. 7a) that is interpreted to reflect the time of protolith emplacement. Four zircon grains of the same sample were evaporated separately and provided a combined mean ^{207}Pb/^{206}Pb age of 2711.1±0.3 (Table 2, Fig. 7a, inset). A slightly younger age was obtained for a medium-grained trondhjemitic gneiss of undoubted granitoid origin (Ch 990838, Table 3), collected in Big Stone Valley at a little waterfall some 100 m W of the village of Quegou (No. 14 in Table 4 and Fig. 2). The zircons are uniformly long-prismatic with well rounded terminations and display well developed oscillatory zoning (Fig. 7b, inset). Six zircon spots analysed on SHRIMP II yielded concordant or near-concordant data with a mean ^{207}Pb/^{206}Pb age of 2701±5.5 Ma (Table 1, Fig. 7b) which we also interpret to reflect the time of protolith emplacement. Two further samples yielded similar but slightly younger results. Grey, homogeneous biotite granite-gneiss sample Ch 980811 of granodioritic composition (Table 3) was collected from a roadcut in Big Stone Valley near the village of Quegou (No. 5 in Table 4 and Fig. 2). The zircons are light yellow-brown, long-prismatic with slightly rounded terminations and good magmatic zoning. Four grains provided a combined mean ^{207}Pb/^{206}Pb evaporation age of 2697.1±0.3 (Table 2, Fig. 8a). Sample 980824 is a finely-layered light grey biotite gneiss of granitic derivation (Table 3) and was collected at a blasted roadcut at the beginning of Great Wall Valley just E of the village of Changchenggou (No. 7 in Table 4 and Fig. 2). The yellow-brown zircons of this sample are less than 100 µm in length, long-prismatic in shape with rounded ends and oscillatory zoning. Several optically identical grains were therefore evaporated together in two experiments, yielding a combined mean ^{207}Pb/^{206}Pb age of 2670.6±0.4 Ma (Table 2, Fig. 8b).

We interpret all the above ages as reflecting the time of emplacement of the igneous protoliths, and these rare ~2670−2710 Ma gneisses may either constitute remnants of a basement to the younger ca. 2500 Ma granitoid generation described below or they may be the oldest part of the same igneous suite to which the ca. 2500 Ma gneisses belong. The intense ductile deformation makes it impossible to identify the original nature and extent of these rocks, but we consider the second alternative unlikely since ages intermediate between ca. 2700 and 2500 Ma have so far not been found, making it unlikely that there was a break of some 200 Ma in magmatic activity within the same magmatic assemblage. We therefore prefer the interpretation that these rocks were derived from an older basement, tectonically sandwiched in between the younger gneisses and flattened together with the enclosing rocks during a severe Palaeoproterozoic ductile deformation event.

The next group of four samples has surprisingly uniform ages in the range 2526–2420 Ma (Table 4, Figs. 7−11) and represents the bulk of the gneissic assemblage in the Hengshan complex. These rocks either exhibit pronounced compositional layering or are homogeneous but well foliated. One of the oldest rocks of this group is a fine-grained leucogneiss (Ch 990821) collected from a blasted roadcut between Taihelingkou and Xinguanwu (No. 13 in Table 4 and Fig. 2) and appearing distinct from the adjacent granite-gneisses by its laminar layering. This rock consists of quartz, plagioclase, minor K-feldspar, and small flakes of hornblende and biotite, and was previously interpreted as a metagreywacke and assigned to the Wutai Group; we interpret it as a metadacite, and the zircon morphology (Fig. 7c, inset) supports this view. Six euhedral, needle-like zircons with well developed oscillatory zoning were analyzed on SHRIMP and provided concordant and near-concordant results with a mean ^{207}Pb/^{206}Pb age of 2526±4.7 Ma (Table 1, Fig. 7c). This age is identical to the felsic rocks of the Wutai Group (Wilde et al., 2000; 2004; see also Kröner et al., 2003), and we tentatively interpret the above rock as representing a felsic volcanic unit, perhaps representing the upper level of the Hengshan magmatic arc or the Wutai felsic suite, that became tectonically interdigitated with the plutonic assemblage.

An identical age was obtained for tonalitic gneiss sample HG 6, collected from a roadcut near Yanmenguan in the western Hengshan (Fig. 2), where 12 SHRIMP analyses (Table 1) yielded a mean ^{207}Pb/^{206}Pb age of 2526 ±12 Ma (Fig. 9b). The third sample of this group is a homogeneous, well foliated but unveined trondhjemitic gneiss (Ch 990847) from the migmatite terrain in the lower part of Big Stone Valley (No. 13 in Table 4 and Fig. 2). The zircons are long-prismatic with rounded ends and good oscillatory zoning. Five grains were analyzed on SHRIMP II of which three are virtually concordant and two are discordant, but all are well aligned, suggesting

Recent Pb-loss and a mean ^{207}Pb/^{206}Pb age of 2524±8 Ma (Table 1, Fig. 7d). Three additional grains were evaporated and produced a mean ^{207}Pb/^{206}Pb age of 2521.7 ±0.4 Ma (Table 2, Fig. 7d, inset), identical to the SHRIMP age, within error. The fourth sample is a garnetiferous trondhjemitic gneiss (HG 5) collected from a fresh roadcut near Yanmenguan in the western Hengshan (Fig. 2) where numerous gabbroic dykes with high-pressure mineralogy cut the orthogneisses (O'Brien et al., 2005). Eleven grains analyzed on SHRIMP (Table 1) provided a mean ^{207}Pb/^{206}Pb age of 2520±10 Ma (Fig. 9a) which we interpret to reflect the age of emplacement of the gneiss precursor. Two idiomorphic grains from the sample are considerably younger, and four SHRIMP analyses (Table 1) yielded a combined mean ^{207}Pb/^{206}Pb age of 1912±9 Ma (Fig. 9a). This age is identical to that of igneous zircons reported from several metagabbroic dyke remnants in the Hengshan (1915±4 Ma, Kröner et al., 2005b), and since such dykes are numerous in the Yanmenguan area we consider it likely that local new zircon growth occurred in some gneisses during dyke emplacement.

The majority of our zircon ages are around 2500 Ma and come from granitoid gneisses ranging in composition from dioritic to granitic. Their location is shown in Fig. 2, and the ages are summarized in Table 4. Some of the migmatitic gneiss varieties in the lower parts of Big Stone and Great Wall Valleys also belong to this age group, as does one sample from the western Hengshan collected from a roadcut SE of Yanmengguan (HG 7, Fig. 9c). The SHRIMP (Table 1) and evaporation (Table 2) ages are graphically shown in Figs. 8 to 11. One of the youngest ages of this group was obtained from a dioritic gneiss collected in Great Wall Valley near the village of Quegou (Ch 990803, No. 12 in Table 4 and Fig. 2). This well foliated rock contains many small melt patches that could not be separated from the sample during zircon separation. Two long-prismatic zircons with well rounded terminations yielded slightly discordant SHRIMP results, combining to a mean ^{207}Pb/^{206}Pb age of 2455±2 Ma (Table 1, Fig. 12a), whereas one stubby, euhedral grain produced a much younger age of 1881±7.5 Ma (Table 1) that we consider to reflect the time of melt patch formation associated with high-grade metamorphism. Metamorphic ages of 1850−1880 Ma are common in the Hengshan and were also determined for metamorphic zircons from high-pressure mafic granulites that originated from gabbroic mafic dykes (O'Brien et al., 2005; Kröner et al., 2005b).

The youngest rock in this group of granitoid orthogneisses is a red migmatitic gneiss (sample Ch 020903) exposed next to a large dolerite dyke in Big Stone Valley (No. 26 in Table 4 and Fig. 2). The zircons are oval to long-prismatic and show well developed oscillatory zoning. Five grains were analyzed on the Beijing

SHRIMP and produced discordant results (Table 1) which are, however, well aligned in the Concordia diagram and yielded an upper intercept age of 2420±20 Ma (mean ^{207}Pb/^{206}Pb age is 2420±3 Ma, see Fig. 12b) which we interpret to reflect the time of protolith emplacement.

The 2526−2420 Ma igneous event in the Hengshan complex produced large volumes of calc-alkaline granitoid rocks and seems to reflect the main phase of igneous activity in the region. This overlaps with of calc-alkaline magmatism in the Wutai complex (Wilde et al., 2000; 2004; Kröner et al., 2005a). Since the youngest rock in this suite, the 2420 Ma gneiss described above, displays the same penetrative ductile fabric as the older gneisses, there is no doubt that the main regional deformation in the Hengshan complex is Palaeoproterozoic.

Further evidence for Palaeoproterozoic deformation comes from well foliated gneisses that yielded zircon ages between 2359 and 2112 Ma (Table 4). A fine-grained, grey, granodioritic gneiss sample Ch 980806 (Table 3) was collected in Big Stone Valley (No. 3 in Table 4 and Fig. 2). Evaporation of three zircons, of similar morphology to those described before, yielded identical ^{207}Pb/^{206}Pb ratios that define a mean age of 2358.7±0.5 Ma (Table 2, Fig. 11d). Reddish, pegmatitic granite gneiss sample HG-4 is exposed near the top of the hill at the high point on the road in Great Wall Valley (No. 25 in Table 4 and Fig. 2) and consists of quartz, K-feldspar, plagioclase and minor biotite. The zircons are long-prismatic and undoubtedly of igneous origin. SHRIMP-dating of 11 grains produced an array of variably discordant data points (Table 1) that can be fitted to a chord intersecting concordia at 2331±36 Ma (Fig. 12c). We interpret this as the emplacement age of the gneiss precursor. An identical age of 2329.7±0.6 Ma (Table 2) was obtained through evaporation of three igneous zircons from layered trondhjemitic gneiss sample Ch 990850 (Table 2, Fig. 11e), also collected in Big Stone Valley (No. 19 in Table 4 and Fig. 2). All these rocks have the same foliation as the enclosing older, layered gneisses.

Two significantly younger ages were found in coarse-grained red granitic material that appears to be the result of anatectic melting in migmatitic gneisses of granitic composition. A sample of pegmatitic material cutting older gneisses in lower Big Stone Valley (Ch 990881, No. 24 in Table 4 and Fig. 2) has a mean ^{207}Pb/^{206}Pb evaporation age of 2248.5±0.5Ma (Fig. 11f). A further sample of red anatectic granite (Ch 990844) from strongly migmatitic and anatectic granite gneiss exposed along the asphalt road in the northwesternmost part of Big Stone Valley (No. 16 in Table 4 and Fig. 2) contains slightly rounded, long-prismatic zircons with excellent magmatic
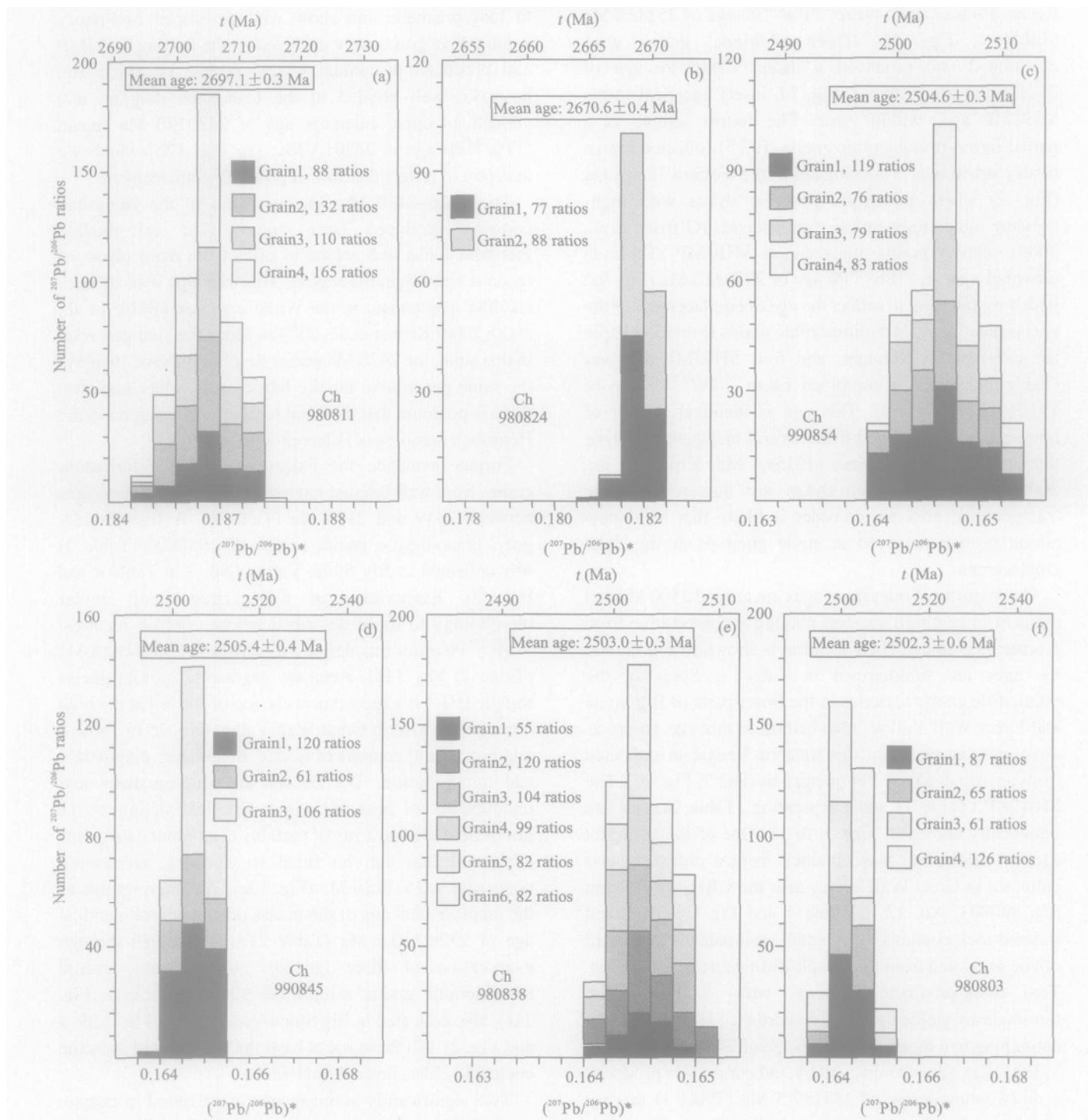
Fig. 8. Histograms showing distribution of radiogenic lead isotope ratios derived from evaporation of single zircons from granitoid gneiss samples of Hengshan Complex, North China Craton. (a) Spectrum for 4 grains from granite gneiss sample Ch 980811, Quegou village, Yinxian area, integrated from 495 ratios. (b) Spectrum for 2 grains from fine-grained biotite gneiss sample Ch 980824, Great Wall Valley, integrated from 165 ratios. (c) Spectrum for 4 grains from trondhjemitic gneiss sample 990854, Ruyueyu valley, integrated from 274 ratios. (d) Spectrum for 3 grains from coarse-grained, well foliated tonalitic gneiss sample Ch 990845, Dashiyu valley, integrated from 287 ratios. (e) Spectrum for 6 grains from trondhjemitic gneiss sample Ch 980838, Ruyueyu valley, integrated from 542 ratios. (f) Spectrum for 3 single zircons from coarse-grained, well foliated tonalitic gneiss sample Ch 980803, Dashiyu valley, integrated from 339 ratios.
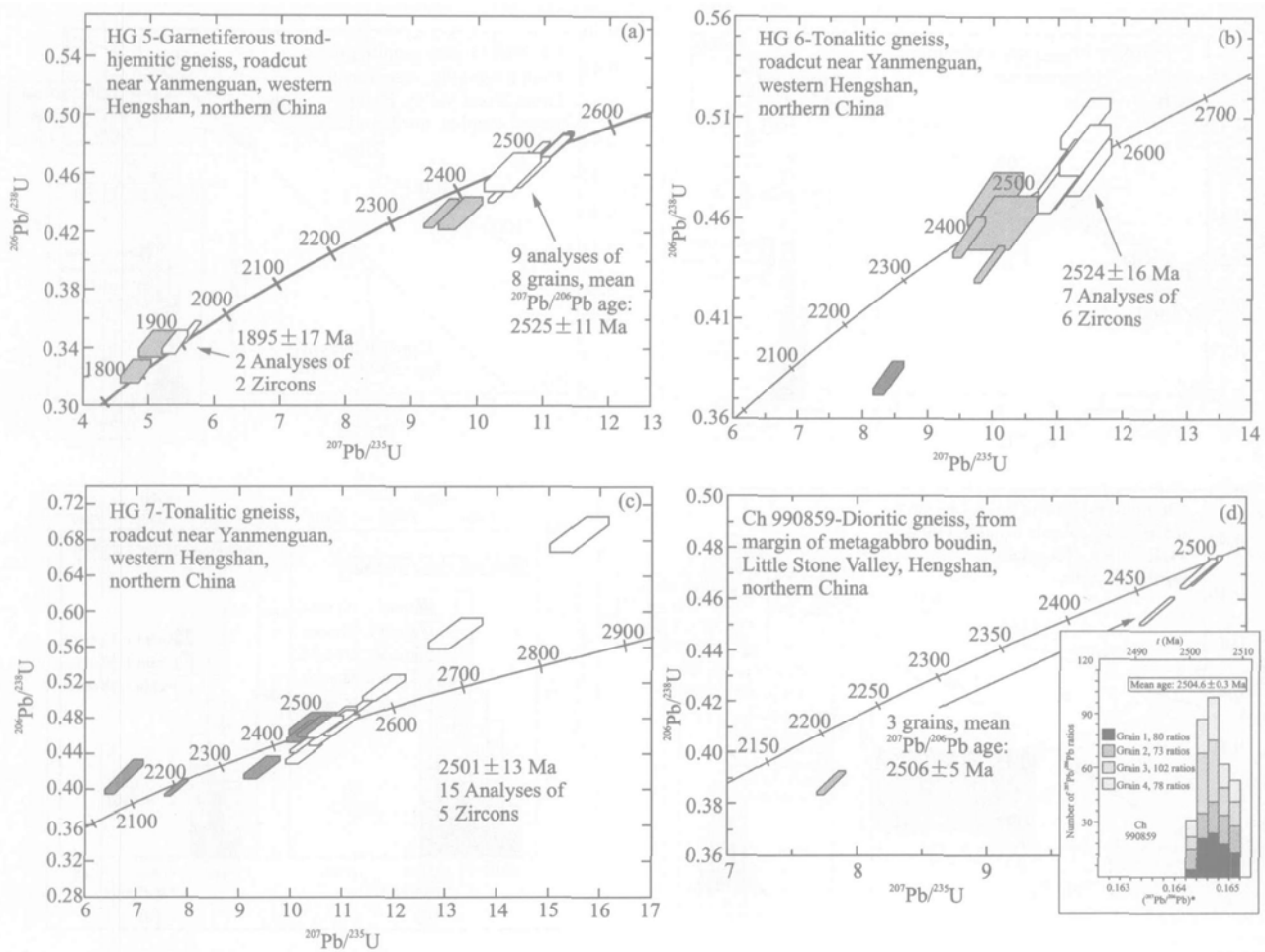
Fig. 9. Concordia diagrams showing SHRIMP analyses of zircons from Hengshan granitoid gneisses, data boxes as in Fig. 7. (a) Garnetiferous trondhjemitic gneiss sample HG 5. Note young age for 2 grains considered to reflect new zircon growth during mafic dyke emplacement. (b) Tonalitic gneiss sample HG 6. (c) Tonalitic gneiss sample HG 7; analysis shaded in grey is from an isotopically disturbed zircon and was not used for age calculation. (d) Dioritic gneiss sample Ch 990859 from margin of large metagabbro boudin. Inset shows histogram with distribution of radiogenic Pb isotope ratios derived from evaporation of 6 single zircons from same sample, integrated from 333 ratios.

zonation (Fig. 12d, inset 1). SHRIMP analysis of four grains produced a concordia upper intercept age of 2113±8 Ma (Fig. 12d), and evaporation of four further grains yielded a mean $^{207}Pb/^{206}Pb$ age of 2112.3±0.6 Ma (Table 2, Fig. 12d, inset 2). We consider it likely that this age reflects the Palaeoproterozoic anatectic event.

Since the youngest rock in this suite, the 2112 Ma gneiss described above, displays the same structural features as the older gneisses, it is obvious that the main D_3 deformational event in the Hengshan complex, producing a penetrative foliation and layering in the gneisses, must post-date this age. This is also supported by a mafic dyke emplacement age of 1915±4 Ma, based on SHRIMP dating of igneous zircons from two dykes in Big Stone Valley (Kröner et al., 2005b). Since these dykes were ductilely deformed and then experienced HP metamorphism, the main deformation event in the

Hengshan complex must be younger than ~1915 Ma. Similar relationships are exposed in the Fuping complex farther southeast where ~2 Ga old granitoids (Zhao et al., 2002) show the same penetrative and ductile deformation as the Hengshan gneisses.

The last event recorded in zircons of the Hengshan terrain is a granulite-facies high-pressure and high-temperature episode, preserved in some of the boudinaged mafic dykes. Details of the metamorphic petrology of these dykes were provided by Liu et al. (1993) and O'Brien et al. (2005). Kröner et al. (2005b) reported zircon ages of 1886 to 1850 Ma for clear, ball-round, multifaceted zircons of undoubted metamorphic origin. A spectacular example of pegmatitic melt generation was found in a large gabbro boudin in Big Stone Valley and probably reflects decompression melting at the end of the high-grade event. Zircons from these melt aggregates were dated at ~1850 Ma (Kröner et al., 2005b).
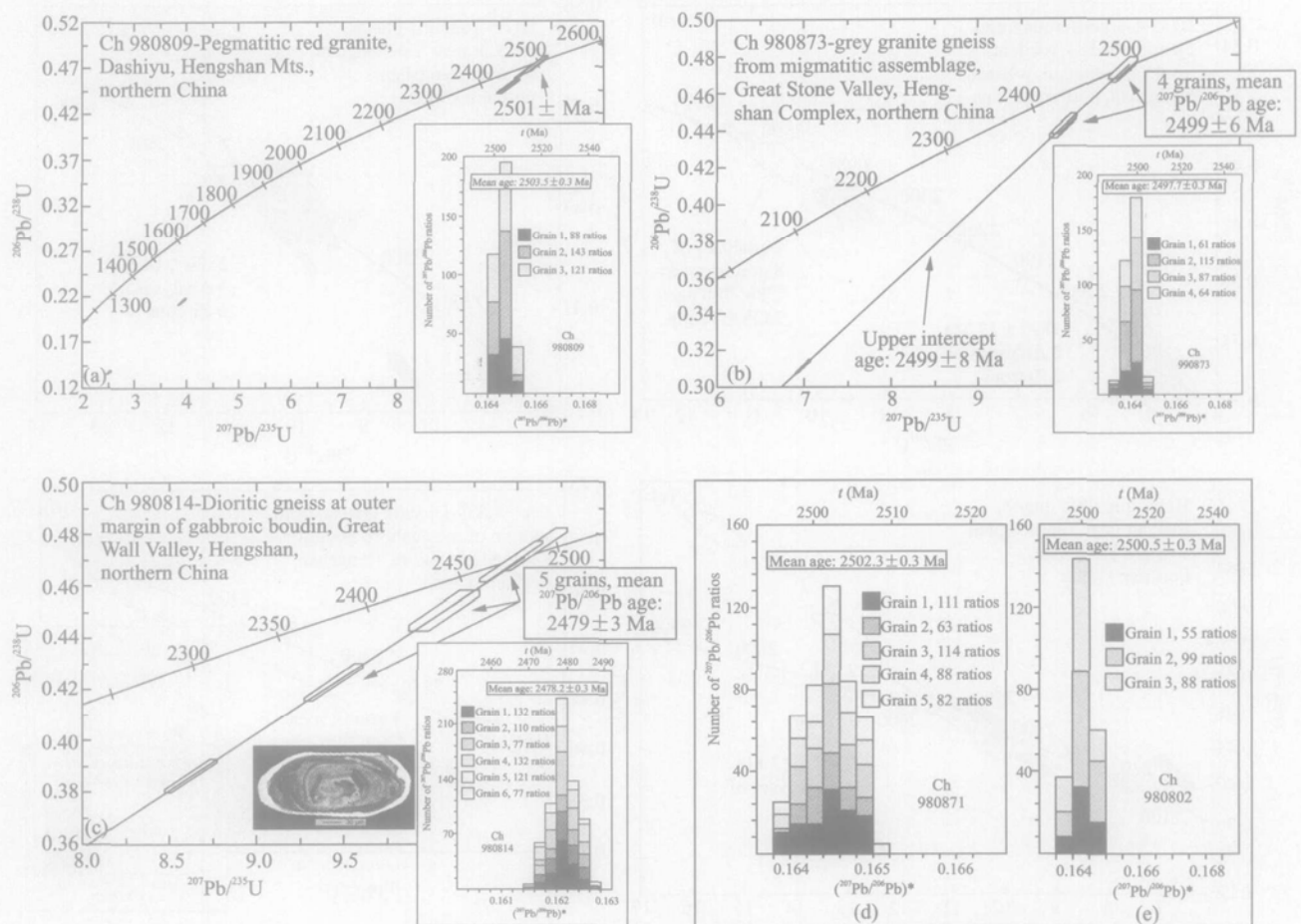
Fig. 10. Concordia diagrams and histograms showing analytical data from SHRIMP and evaporation analysis of single zircons from granitoid gneiss samples of Hengshan Complex, North China Craton. Error symbols in (a) to (c) as in Fig. 7. (a) Pegmatitic red granite gneiss sample Ch 980809. Inset shows histogram with distribution of radiogenic Pb isotope ratios derived from evaporation of 4 single zircons from same sample, integrated from 432 ratios. (b) Migmatitic grey granodioritic gneiss sample Ch 990873. Inset shows histogram with distribution of radiogenic Pb isotope ratios derived from evaporation of 4 single zircons from same sample, integrated from 327 ratios. (c) Dioritic gneiss sample Ch 980814 from outer margin of gabbroic granulite boudin. Inset 1 shows CL-image of oszillatory-zoned magmatic zircon with thin U-poor (metamorphic?) overgrowth. Inset 2 shows histogram with distribution of radiogenic Pb isotope ratios derived from evaporation of 6 single zircons from same sample, integrated from 649 ratios. (d) Spectrum for radiogenic lead isotope ratios derived from evaporation of 5 zircons from foliated tonalite sample Ch 990871, Ruyueyu Valley, integrated from 458 ratios. (e) Spectrum for radiogenic lead isotope ratios derived from evaporation of 3 zircons from tonalitic gneiss sample Ch 980802, S of Xiaheyu village, Big Stone Valley, integrated from 242 ratios.

7 Discussion and Tectonic Model

The main mass of the Hengshan granitoid suite, dated between ~2525 and ~2420 Ma, was probably generated in the lower levels of a Japan-type magmatic arc (Kay and Mahlburg-Kay, 1991). The existence of pre-arc continental basement of unknown tectonic affinity is shown by the occurrence, albeit rare, of ~2670–2710 Ma granitoid gneisses. Similarly rare gneisses of this age were also described from the Fuping complex farther SE (Guan et al., 2002; Zhao et al, 2002). These rocks provide evidence for the existence of a continental terrane whose relation with rocks of similar or older age in northern

China is unknown. We therefore tentatively interpret this as part of a microcontinent of unknown dimensions and origin or, more likely, as the westernmost part of the Eastern block of the North China Craton.

Geochemically, both the Hengshan and Fuping gneisses are similar to Archaean TTG-suites elsewhere is the world (e.g. Martin, 1987) that have been interpreted as root zones of arc complexes (e.g. Cassidy et al., 1991; Percival, 1994). Liu et al. (2002) provided geochemical and isotopic data showing the Fuping TTG gneisses to be the result of mixing of mantle-derived melts related to a major underplating event at ~2.5 Ga with older crust characterized by Nd-model ages of 2.8−3.0 Ga.

The geochemical features of felsic to intermediate
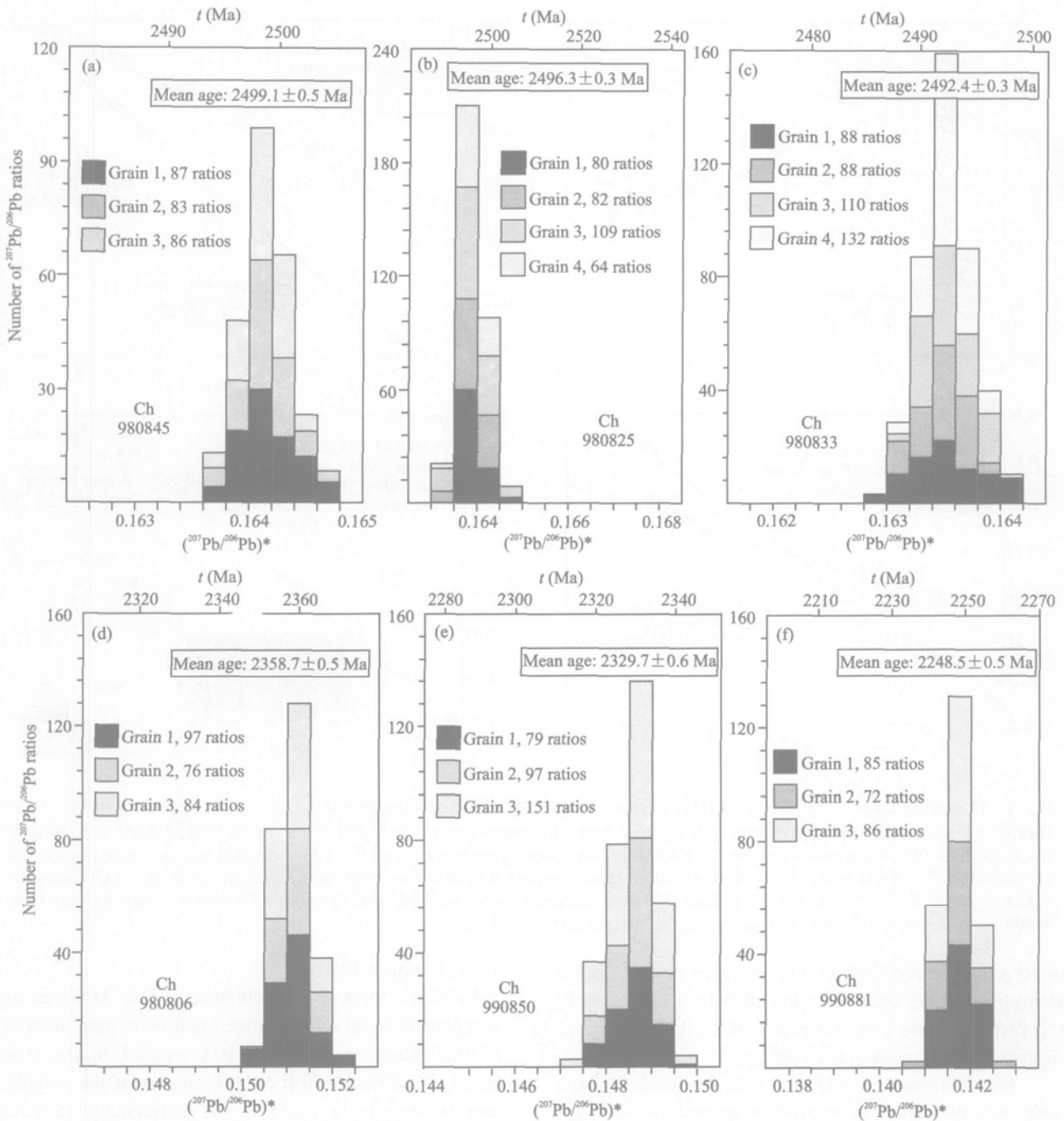
Fig. 11. Histograms showing distribution of radiogenic lead isotope ratios derived from evaporation of single zircons from granitoid gneiss samples of Hengshan Complex, North China Craton. (a) Spectrum for 3 zircon grains from leucocratic granitoid gneiss sample Ch 980845 in outer zone of mafic boudin, Little Stone Valley, integrated from 256 ratios. (b) Spectrum for 4 zircon grains from tonalitic gneiss sample Ch 980825, S of Xiaheyu village, Big Stone Valley, integrated from 335 ratios. (c) Spectrum for 4 zircon grains from leucocratic granite-gneiss sample Ch 980833 in outer zone of mafic boudin, Little Stone Valley, integrated from 418 ratios. (d) Spectrum for 3 zircon grins from coarse pegmatitic red granite sample Ch 980806, Big Stone Valley, integrated from 257 ratios. (e) Spectrum for 3 zircon grains from coarse-grained pegmatitic red granite sample 990850, Big Stone Valley, integrated from 327 ratios. (b) Spectrum for 3 zircon grains from pegmatite sample 990881, road cut in Big Stone Valley, integrated from 243 ratios.

metavolcanic rocks of the upper crustal Wutai complex situated SE of the Hengshan (Fig. 1) are also remarkably similar to those of the Hengshan and Fuping gneisses (Wilde et al., 2004) and, together with their almost identical ages to those of the Hengshan and Fuping, make a strong case for our interpretation that the Wutai is the upper crustal equivalent of the lower to middle crustal Hengshan-Fuping granitoid suite and that all these rocks
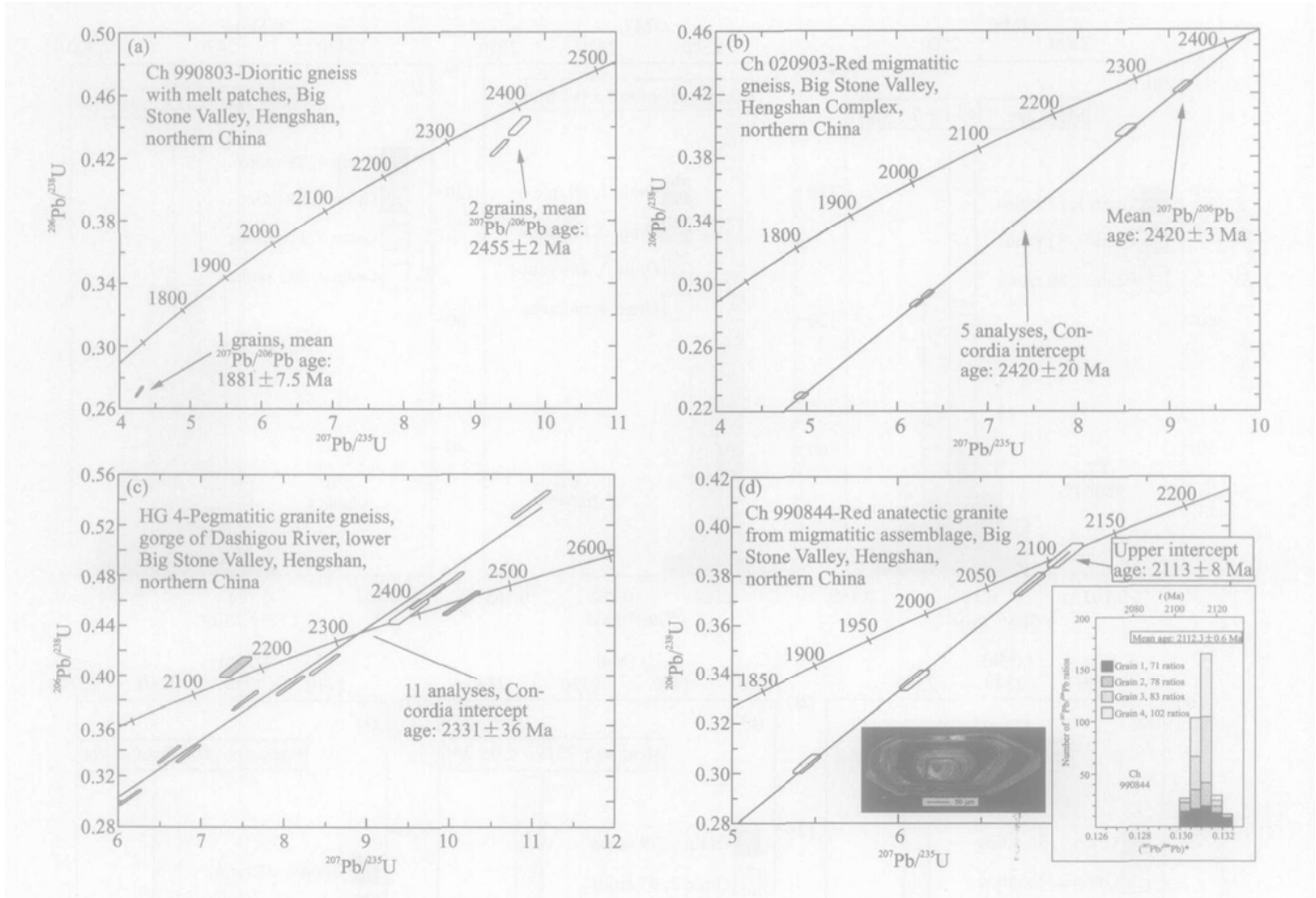
Fig. 12. Concordia diagrams showing SHRIMP analyses of zircons from Hengshan granitoid gneisses, data boxes as in Fig. 7. (a) Dioritic gneiss sample Ch 990803 with melt patches. Most discordant grain with $^{207}Pb/^{206}Pb$ age of 1881±7.5 Ma is from melt patch. (b) Red migmatitic gneiss sample Ch 020903. (c) Pegmatitic granite gneiss sample HG 4. Shaded analyses were not used in calculation of Concordia intercept. (d) Red anatectic granite sample Ch 990844 from migmatitic assemblage. Inset 1 is CL-image of euhedral zircon with oszillatory zoning. Inset 2 shows histogram with distribution of radiogenic Pb isotope ratios derived from evaporation of 4 single zircons from same sample, integrated from 649 ratios.

together constitute a crustal profile through a Japan-type magmatic arc (Kröner et al., 2005a)

The voluminous ~2525 − 2420 Ma Hengshan plutonic suite was produced by subduction-related calc-alkaline magmatism (Liu et al., 2003) in a lower crustal environment, and these were the precursors of the present gneisses. Kröner et al. (2005a) speculated that these rocks, together with felsic, intermediate and mafic volcanic assemblages of the Wutai complex and associated high-level granites, generated a magmatic arc along the active margin of the above microcontinent or Eastern block of the NCC (Fig. 13a). Some of the ~2.7 Ga basement was remelted during this event and contributed crustal material to the arc magmas, now seen as xenocrystal zircons in the gneisses and metavolcanic rocks (Fig. 13b). The time range of ~100 m.a. for the generation of these rocks is comparable to the generation of Archaean and Palaeoproterozoic arcs elsewhere in the world (Goodwin,

1991; Windley, 1995).

Evidence for early deformation of late Archaean age and generation of a penetrative foliation in tonalitic rocks of the Hengshan complex, is preserved in low-strain zones, in particular in the southern part of the complex, and is tentatively ascribed to accretionary tectonics, probably associated with deformation along the evolving active margin of the arc terrane. It is likely that the original crustal structure of the arc was already affected by this deformation, and rocks generated at different crustal levels became tectonically interdigitated and/or juxtaposed.

Volumetrically much less significant granitoid magmatism continued through the early Palaeoproterozoic in the Hengshan, particularly at ~2360−2330 Ma, 2250 Ma and 2115 Ma (Table 4). Some of these are anatectic melts, as seen from field relationships, and are therefore likely to be related to crustal thickening events. It is particularly important to note that the granitoids emplaced
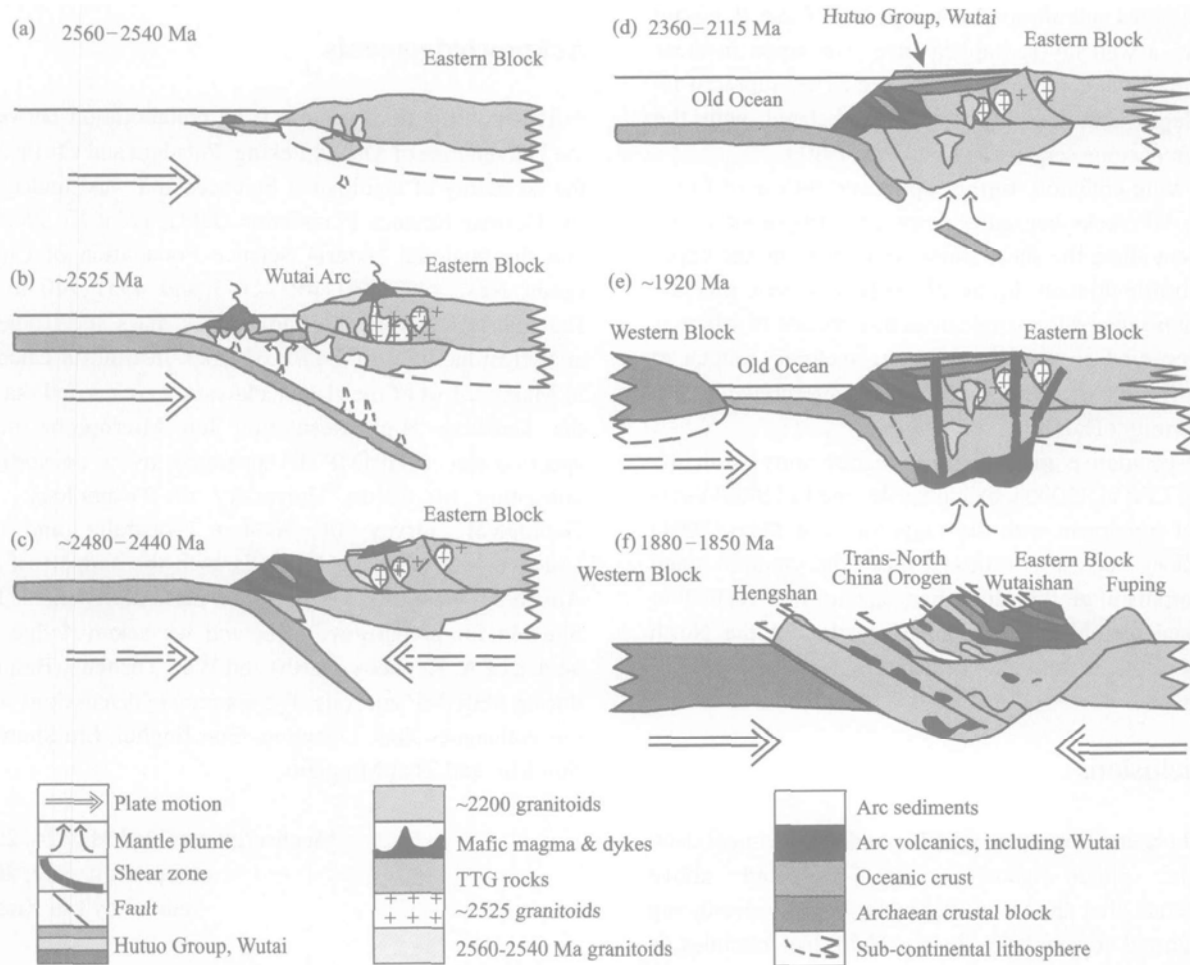
Fig. 13. Tectonic model for the evolution of the Hengshan-Wutaishan-Fuping crustal section (adapted from Kröner et al., 2005a). For explanation see text.

at 2360−2115 Ma in the Hengshan complex contain the same deformational features as the older gneisses and thus unambiguously demonstrate that the main deformational event is not Archaean but Palaeoproterozoic in age.

The next stage is seen in the emplacement of a mafic dyke swarm at ~1920 Ma (Kröner et al., 2005b) (Fig. 13e), now preserved as boudinaged gabbroic dykes and sills. In the southern Hengshan complex these dykes intruded into already foliated tonalitic gneisses. Similar dykes occur in the Wutai and Fuping complexes farther SE, and this dyke swarm signifies an extensional event of regional proportions. Mafic dyke emplacement also constitutes an older age limit to the main fabric-forming event in the Hengshan. The long time interval of ~600 Ma between emplacement of the main volume of granitoid rocks at about 2500 Ma and intrusion of the mafic dyke swarms at ~1900 Ma suggests that there is no genetic relationship between arc formation at the end of the Archaean and crustal extension and rifting initiating the Lüliang orogenic event in the Palaeoproterozoic.

The main deformation event leading to a penetrative ductile fabric in the Hengshan granitoid rocks took place after mafic dyke emplacement, most likely at the same time when high-pressure metamorphism occurred at 1880 −1850 Ma that is recorded in numerous gabbroic dykes which were described as mafic granulites (Li et al, 1998b; Zhao et al., 2001a; O'Brien et al., 2005). We relate this to a major collision event reflected by compressional structures and a clockwise *P-T* path in the Hengshan granulites (Zhao et al., 2001a) during formation of the Trans-North China orogenic belt when the western and eastern blocks of the NCC collided (Zhao, 2001) (Fig. 13e) and the overall structure of the Hengshan/Fuping/ Wutai magmatic arc was finally destroyed and the rocks were tectonically interdigitated (Kröner et al., 2005a). This is the Lüliang orogeny of the Chinese literature. Collision-induced intracrustal thrusting transported the Hengshan and Fuping granitoid assemblages into lower crustal levels where ductile deformation prevailed (Fig. 13f). Subsequent uplift as a result of orogenic collapse generated major shear zones in the lower crustal domains in which many of the granitoid gneisses were transformed

into mylonites and ultramylonites, at high T and P, giving the rocks a well layered appearance. The rocks in these shear zones were mistakenly interpreted as supracrustal assemblages and were previously correlated with the Wutai greenstone sequence (e.g., Tian, 1991).

Following collision, further uplift and inflow of fluids into the HP rocks caused widespread retrogression, and movement along the shear zones continued into the upper crustal brittle domain. In the Wutai/Fuping area, this late shearing produced low-angle detachments one of which is now preserved as the Wutai/Fuping tectonic contact at Tiebao (Li et al., 2003), previously interpreted as an unconformity (Tian et al., 1996).

Our speculative model differs significantly from the views of Li et al. (2000a, b) and Kusky and Li (2003) but is in broad agreement with the suggestions of Zhao (2001) and Zhao et al. (2004) that deformation and metamorphism of the Hengshan terrain was related to collisional tectonics during amalgamation of the North China Craton in the early Proterozoic some 1880−1850 Ma ago.

8 Conclusions

Field observations, petrographic and geochemical data, and the zircon geochronology presented above demonstrate that the main magmatic activity producing the granitoid assemblages in the Hengshan complex is latest Archaean to Palaeoproterozoic in age (~2526−2115 Ma) and is thus similar in age to other parts of the North China Craton (e.g., Ren et al., 1987; Liu et al., 1990; Kröner et al., 1998, Zhao et al., 2001), including the adjacent Wutai and Fuping complexes. Rare remnants of what may be an older basement are present as small, discontinuous domains of ~2700 Ma rocks that are tectonically sandwiched in between the younger gneisses. The main event of ductile deformation and high-grade metamorphism giving rise to the conspicuous layering and flattening in most rocks in the Hengshan complex, including the formation of a HP-metamorphic assemblage, is ca. 1850 − 1880 Ma in age and post-dates the emplacement of the ~1920 Ma gabbroic dykes.

Our data do not support models of late Archaean cratonization in northern China but reflect extensive Palaeoproterozoic tectonism and metamorphism, probably related to amalgamation of several Archaean crustal domains, the oldest nucleus of which was probably in eastern Hebei (Liu et al., 1990). Thus, the Lüliang orogeny probably was one of the most important events in the history of the NCC, welding together older domains and similar to the Trans-Hudson orogeny of the Canadian shield (Maxeiner et al., 2004).

References

Bai, J., 1986. The Precambrian crustal evolution of the Wutaishan area. In: Bai, J. (ed.), *The Early Precambrian Geology of Wutaishan*. Tianjin: Tianjin Science and Technology Press, 376−383 (in Chinese).

Cassidy, K.F., Barley, M.E., Groves, D.I., Perring, C.J., and Hallberg, J.A., 1991. An overview of the nature, distribution and inferred tectonic setting of granitoids in the late Archean Norseman-Wiluna belt. *Precambrian Res.*, 51: 51−83.

Claoué-Long, J.C., Compston, W., Roberts, J., and Fanning, C.M., 1995. Two Carboniferous ages: a comparison of SHRIMP zircon dating with conventional zircon ages and $^{40}Ar/^{39}Ar$ analysis. In: Geochronology time scales and global stratigraphic correlation. *SEPM Special Publication*, 54: 3−20.

Cocherie, A., Guerrot, C., and Rossi, P.H., 1992. Single-zircon dating by stepwise Pb evaporation: Comparison with other geochronological techniques applied to the Hercynian granites of Corsica, France. *Chemical Geol.*, 101: 131−141.

Cumming, G.L., and Richards, J.R., 1975. Ore lead isotope ratios in a continuously changing earth. *Earth Planet. Sci. Lett.*, 28: 155−171.

DeBari, S.M., and Sleep, N.H., 1991. High-Mg, low-Al bulk composition of the Talkeetna island arc, Alaska: Implications for primary magmas and the nature of arc crust. *Geol. Soc. Am. Bull.*, 103: 37−47.

DeBari, S.M., Anderson, R.G., and Mortensen, J.K., 1999. Correlation among lower to upper crustal components in an

island arc: the Jurassic Bonanza arc, Vancouver Island, Canada. *Canadian J. Earth Sci.*, 36: 1371–1413.

Debon, F., and Le Fort, P., 1983. A chemical-mineralogical classification of common plutonic rocks and associations. *Trans. Roy. Soc. Edinburgh, Earth Sci.*, 73: 135–149.

De Laeter, J.R., and Kennedy, A.K., 1998. A double focusing mass spectrometer for geochronology. *Intl. J. Mass Spectrometry*, 178: 43–50.

England, P.C., and Richardson, S.W., 1977. The influence of erosion upon the mineral facies of rocks from different metamorphic environments. *J. Geol. Soc. London*, 134: 201–213.

Goodwin, A.M., 1991. *Precambrian Geology—The Dynamic Evolution of the Continental Crust*. Toronto: Academic Press, 666.

Guo, J.H., Zhai, M.G., and Li, Y., 1994. Isotopic ages and their tectonic significance of metamorphic rocks from middle part of the early Precambrian granulite belt, North China craton. In: Qian, X.L., and Wang, R.M. (eds.), *Geological Evolution of the Granulite Terranes in the North Part of the North China Craton*. Beijing: Seismological Press, 120–129 (in Chinese with English abstract).

Halls, H.C., Li, J.H., Davis, D., Hou, G.T., Zhang, B.X., and Qian, X.L., 2000. A precisely dated Proterozoic paleomagnetic pole from the North China craton and its relevance to paleocontinental reconstruction. *Geophys. J. Intl.*, 143: 185–203.

Harris, N.B.W., Pearce, J.A., and Tindle, A.G., 1986. Geochemical characteristics of collision-zone magmatism. In: Coward, M.P., Ries, A.C. (eds.), *Collision Tectonics*. Geological Society of London, Special Publication, 19: 67–81.

Hoskin, P.W.O., and Black, L.P., 2000. Metamorphic zircon formation by solid-state recrystallization of protolith igneous zircon. *J. Metamorphic Geol.*, 18: 423–439.

Jaeckel, P., Kröner, A., Kamo, S.L., Brandl, G., and Wendt, J.I., 1997. Late Archaean to early Proterozoic granitoid magmatism and high-grade metamorphism in the central Limpopo belt, South Africa. *J. Geol. Soc. London*, 154: 25–44.

Karabinos, P., 1997. An evaluation of the single-grain zircon evaporation method in highly discordant samples. *Geochimi. Cosmochim. Acta*, 61: 2467–2474.

Kay, R.W., and Mahlburg-Kay, S., 1991. Creation and destruction of lower continental crust. *Geologische Rundschau*, 80: 259–278.

Kinny, P.D., 1986. 3820 Ma zircons from a tonalitic Amitsoq gneiss in the Godthab district of southern West Greenland. *Earth Planet. Sci. Lett.*, 79: 337–347.

Kröner, A., 1998. Evolution of high-grade gneisses in the Central Zone of the Limpopo belt, South Africa, and the Jianping Complex, Liaoning Province, China: Similarities and differences, and significance for crustal evolution. In: Collected works of International Symposium on Geological Science at the occasion of the 100th Anniversary of Peking University. Department of Geology, Peking University, 317–333.

Kröner, A., Byerly, C.R., and Lowe, D.R., 1991. Chronology of early Archean granite-greenstone evolution in the Barberton Mountain Land, South Africa, based on precise dating by single zircon evaporation. *Earth Planet. Sci. Lett.*, 103: 41–54.

Kröner, A., and Hegner, E., 1998. Geochemistry, single zircon ages and Sm-Nd systematics of granitoid rocks from the Góry Sowie (Owl) Mts., Polish West Sudetes: evidence for early Palaeozoic arc-related plutonism. *J. Geol. Soc. London*, 155: 711–724.

Kröner, A., Jaeckel, P., Brandl, G., Nemchin, A.A., and Pidgeon, R.T., 1999. Single zircon ages for granitoid gneisses in the Central Zone of the Limpopo belt, southern Africa, and geodynamic significance. *Precambrian Res.*, 93: 299–337.

Kröner, A., O'Brien, P.J., Li, J.H., Passchier, C.W., and Wilde, S., 2000. Chronology, metamorphism and deformation in the lower crustal Hengshan complex and significance for the evolution of the North China Craton. *Abstract-volume*, 32nd International Geological Congress, Rio de Janeiro, Brazil.

Kröner, A., Zhao, G.C., Wilde, S.A., Zhai, M.G., Passchier, C.W., Sun, M., Guo J.H., O'Brien, P.J., and Walte, N. (Comp.), 2002. A late Archaean to Palaeoproterozoic lower to upper crustal section in the Hengshan-Wutaishan area of North China. *Penrose Conference Guidebook for field trip*. Beijing: Chinese Academy of Sciences.

Kröner, A., Wilde, S.A., Li, J.H., Wang, K.Y., and Zhao G.C., 2005a. Age and evolution of a late Archaean to early Palaeoproterozoic upper to lower crustal section in the Wutaishan/Hengshan/Fuping terrain of northern China. *J. Asian Earth Sci.*, 24: 577–595.

Kröner, A., Zhao G.C., Sun, M., Liu, D.Y., and Wan Y.S., 2005b. Emplacement age for mafic dykes (HP granulites) in the Hengshan metamorphic complex, North China craton, and implication for Palaeoproterozoic tectonics. *Precambrian Res.* (in press).

Kusky, T.M., and Li, J.H., 2003. Paleoproterozoic tectonic evolution of the North China craton. *J. Asian Earth Sci.*, 22: 23–40.

Kutsukake, T., 2002. Geochemical characteristics and variations of the Ryoke granitoids, southwest Japan: Petrogenetic implications for the plutonic rocks of a magmatic arc. *Gondwana Research*, 5: 355–372.

Li, J.H., and Qian, X.L., 1991. A study of Longquanguan shear zone in the northern part of the Taihang Mountain. *Shanxi Geology*, 6: 17–29 (in Chinese).

Li, J.H., and Qian, X.L., 1994. *The Early Precambrian Crustal Evolution of Hengshan Metamorphic Terrain, North China Craton*. Xi'an: Shanxi Science and Technology Press, 124 (in Chinese with extended English abstract).

Li, J.H., Qian, X.L., and Zhai, M.G., 1997. Tectonic division of the North China granulite facies belt and its early Precambrian tectonic evolution. *Sci. Geol. Sinica*, 32: 254–266.

Li, J.H., Zhai, M.G., and Li, Y.G., 1998a. Discovery of Neoarchean high-pressure granulites in Luanping-Chengde area, Northern Hebei, and their tectonic-geological implications. *Acta Petrol. Sinica*, 14: 34–41.

Li, J.H., Zhai, M.G., and Qian, X.G., 1998b. The geological occurrence, regional tectonic setting and exhumation of late Archaean high-pressure granulite within the high-grade metamorphic terrains, north to central portion of North China Craton. *Acta Petrol. Sinica*, 14: 176–189.

Li, J.H., Qian, X.L., Huang, X.N., and Liu, S.W., 2000. The tectonic framework of the basement of North China craton and its implications for early Precambrian cratonization. *Acta Petrol. Sinica*, 16: 1–10.

Liu, D.Y., Shen, Q.H., Zhang, Z.Q., Jahn, B.M., Auvray, B., 1990. Archean crustal evolution in China: U-Pb geochronology of the Qianxi Complex: *Precambrian Res.*, 48: 223 − 244.

Liu, X.S., Jin, W., Li, S.X., Xu, X.C., 1993. Two types of Precambrian high-grade metamorphism, Inner Mongolia, China. *J. Metamorphic Geol.*, 11: 499 − 510.

Liu, S.W., Li, J.H., Pan, Y.M., Zhang, J., Li, Q., 2002. An Archean continental block in the Taihangshan and Hengshan regions: constraints from geochronology and geochemistry. *Progress Natural Sci.*, 12: 568 − 576.

Liu, S.W., Pan, Y.M., Xie, Q.L., Zhang, J., and Li, Q.G., 2004. Archean geodynamics in the Central Zone, North China craton: constraints from geochemistry of two contrasting series of granitoids in the Fuping and Wutaishan complexes. *Precambrian Res.*, 130: 229 − 249.

Ludwig, K. R., 1999. User's Manual for Isoplot/EX version 2.2. *A Geochronological Toolkit for Microsoft Excel*. Berkeley Geochronology Center Special Publication 1a, 53.

Ma, X.Y., Bai, J., Suo, S.T., Lao, Q.Y., and Zhang J.S., 1987. *The Precambrian Tectonic Framework and the Research Method in China*. Beijing: Geological Publishing House (in Chinese with English abstract).

Ma, X.Y., and Bai, J. (eds.), 1998. *Precambrian Crustal Evolution of China*. Beijing: Springer Geological Publishing, 331.

Martin, H., 1987. Evolution in composition of granitic rocks controlled by time-dependent changes in petrogenetic processes: examples from the Archean of eastern Finland. *Precambrian Res.*, 35: 257−276.

Maxeiner, R.O., Corrigan, D., Harper, C.T., MacDougall, D.G., Ansdell, K., 2004. Palaeoproterozoic arc and ophiolitic rocks on the northwest-margin of the Trans-Hudson orogen, Saskatchewan, Canada: their contribution to a revised tectonic framework of the orogen. *Precambrian Res.*, 136: 67−106.

Myers, J. S., 1978. Formation of banded gneisses by deformation of igneous rocks. *Precambrian Res.*, 6: 43−64.

Nelson, D. R., 1997. *Compilation of SHRIMP U-Pb Zircon Geochronology Data*, *1996*. Geological Survey of Western Australia, Record 1997/2, 189.

O'Brien, P.J., Walte, N., and Li, J.H., 2005. The petrology of two distinct Paleoproterozoic granulite types in the Hengshan Mts., North China craton, and tectonic implications. *J. Asian Earth Sci.*, 24: 615−628.

Passchier, C. W. Myers, J.S., and Kröner, A., 1990. *Field Geology of High-grade Gneiss Terrains*. Berlin: Springer-Verlag, 150.

Pearce, J.A., Harris, N.B.W., and Trindle, A.G., 1984. Trace element discrimination diagrams for the tectonic interpretation of granitic rocks. *J. Petrol.*, 25: 956−983.

Percival, J.A., 1994. Archean high-grade metamorphism. In: Condie, K.C. (ed.), *Archean Crustal Evolution*. Amsterdam: Elsevier, 357−410.

Tian, Y.Q, 1986. A preliminary discussion on the geological features and genesis of gray gneisses in Hengshan region. *Shanxi Geology*, 1: 96−112 (in Chinese with English abstract).

Tian, Y.Q., Liang, Y.F., Fan Sikun, Zhu B.Q., and Chen, Y.W., 1992. Geochronology of the Henshan Complec in special reference to Nd isotopic evolution. *Geochimi.*, 9: 255−264 (in Chinese with English abstract).

Tian Y.Q., Ma, Z.H., Yu K.R., Liu, Z.H., and Peng, Q.M., 1996.

The Early Precambrian Geology of Wutai-Hengshan Mts., Shanxi, China. *Field Trip Guide T315*. 30th International Geological Congress, Beijing, China. Beijing: Geological Publishing House, 52.

Viana, M.G., Pimentel, M.M., Whitehouse, M.J., Fuck, R.A., and Machado, N., 1995. O arco magmático de Mara Rosa, Goiás: dados geoquímicos e geocronológicos e suas implicacoes regionais. *Revista Brasiliensis Geociencias*, 25: 111−123.

Walte, N.P., 2001. Metamorphose und Texturentwicklung von Granuliten aus dem Hengshan, Nordchina Kraton. Unpubl. Diploma-thesis, University of Mainz, Germany, 82.

Wang, R.M., Chen, Z.Z., Chen, F., 1991. Grey tonalitic gneiss and high-pressure granulite inclusions in Hengshan, Shanxi Province, and their geological significance. *Acta Petrol. Sinica*, 7: 36−45 (in Chinese with English abstract).

Wilde, S.A., Cawood, P.A., Wang, K.Y., and Nemchin, A., 1998. SHRIMP U-Pb zircon dating of granites and gneisses in the Taihangshan-Wutaishan area: implications for the timing of crustal growth in the North China craton. *Chinese Sci. Bull.*, 43: 144−145.

Wilde, S.A., Cawood, P.A., Wang, K.Y., Nemchin, A., and Zhao, G.C. 2004. Determining Precambrian crustal evolution in China: a case-study from Wutaishan, Shanxi Province, demonstrating the application of precise SHRIMP U-Pb geochronology. In: Malpas, J., Fletcher, C.J.N., Ali, J.R., and Aitchison, J.C. (eds), *Aspects of the Tectonic Evolution of China*. Geological Society of London. Special Publication, 226: 5−25.

Windley, B.F., 1995. The Evolving Continents (3rd edition). Chichester, John Wiley & Sons, 526.

Xie, Q., Jain, J., Sun, M., Kerrich, R., and Fan, J., 1994. Multiple element analysis of low abundance international reference material BIR-1: Results by ICP-MS. *Geostandards Newsletter*, 18: 53−63.

Zhai, M.G., 1997. Recent advances in the study of granulites from the North China craton. *Intl. Geol. Rev.*, 39: 325−341.

Zhai, M.G., and Liu, W.J., 2003. Palaeoproterozoic tectonic history of the North China craton; a review. *Precambrian Res.*, 122: 183−199.

Zhao, G.C., Wilde, S.A., Cawood, P.A., and Li, L.Z., 1999a. Tectonothermal history of the basement rocks in their western zone of the North China Craton and its tectonic implications. *Tectonophysics*, 310: 37−53.

Zhao, G.C., Wilde, S.A., Cawood, P.A., and Lu L.Z., 1999b. Thermal evolution of two textural types of mafic granulites in the North China Craton: evidence for both mantle plume and collisional tectonics. *Geol. Magazine*, 136: 223−240.

Zhao, G.C., Wilde, S.A., Cawood, P.A., and Sun, M., 2001. Archean blocks and their boundaries in the North China Craton: lithological, geochemical, structural and *P-T* path constraints and tectonic evolution. *Precambrian Res.*, 107: 45 −73.

Zhao, G.C., Wilde, S.A, Cawood, P.A., Sun, M., 2002. SHRIMP U-Pb zircon ages of the Fuping Complex: implications for accretion and assembly of the North China Craton. *Am. J. Sci.*, 302: 191−226.

Zhao, G., Sun, M., Wilde, S.A., Li, S., 2004. Late Archean to Paleoproterozoic evolution of the North China Craton: key issues revisted. *Precambrian Res.*, 136: 177−202.